The importance of mineralogy in the formation of polygonal fault systems in the North Sea

How clay mineralogy and the presence of biogenic silica impact the formation of polygonal fault systems

Daniel Vedaa

Master thesis in Geodynamics and Basin Studies

Department of Earth Science

University of Bergen

June 2023

Abstract

Many different theories have been proposed as possible formation mechanisms for polygonal fault systems. Some of these theories suggest volumetric contraction and dewatering of sediments is the mechanism that causes the formation of polygonal faults in line-grained sedimentary lithologies. In this thesis we investigate what influence clay mineralogy, and the presence of biogenic silica has on the North Sea sedimentary sequences known to host polygonal fault systems The focus is primarily on two sequences that represent the Upper and Lower Oligocene sedimentary sequence in the study area in the northern North Sea. These investigations were carried out using available well logs and mineralogy data for the Cenozoic sequences in the northern North Sea basin.

Acknowledgements

This study was conducted as part of my MSc degree at the Department of Earth Science at the University of Bergen. Many have provided both assistance and advice during this project, and I wish to offer my thanks.

First, I would like to express my gratitude to my supervisor Christian Hermanrud and thank him for all the genuine advice and assistance he has provided throughout this study. He was genuinely interested in discussing the topics of the study, and always willing to engage in discussions and provide helpful feedback.

I would also like to thank Philipp Müller, for providing a lot of help with technical challenges related to seismic and well data, and as well for teaching me and fellow students in the use of Petrel and other software.

I want to like to thank everyone the PESTOH study group, for being good company and for the many hours of interesting talks and discussions.

Finally, I want to thank my closest family, for always being supportive and being there for me over many years.

Bergen, June 2023

Daniel Vedaa

Innhold

1. Introduction 1
2. Geological and theoretical background 3
2.1 Geological history and setting 3
2.1.1 The Pre-Cenozoic 3
2.2 Polygonal fault systems 3
2.2.1 Description of polygonal fault systems 3
2.2.2 Suggested formation mechanisms of polygonal fault systems 6
2.3 Opal-A to Opal-CT transformation 11
3. Data and methods 12
3.1 Seismic data 12
3.2 Mineralogy data 15
3.2.1 Uncertainties 18
3.3 Wells and well logs 19
4. Observations and results 22
4.1 Mineralogy observations 22
4.1.1 Clay mineralogy of Well 30/3-3 22
4.1.2 Clay mineralogy of Well 31/2-5 25
4.1.3 Clay mineralogy of well 31/2-1 28
4.1.4 Clay mineralogy of well 31/2-2 30
4.1.5 Clay mineralogy of Well 31/3-1 32
4.1.6 Clay mineralogy of well 34/2-2 34
4.1.7 Clay mineralogy of well 35/3-2 36
4.2 Opal A – Opal-CT diagenetic reflectors & wireline logs 38
4.2.1 Well log for 30/3-3 38
4.2.2 Well log for 31/2-5 40
4.2.3 Well log for 31/4-3 42
4.2.4 Well log for 35/11-3 44
4.2.5 Well log for 31/2-1 46
4.3 Seismic observations 47
4.3.1 Seismic line 1 48
4.3.2 Seismic line 2 49
4.3.3 Seismic line 3 50
5. Interpretation 51
6. Conclusion 53
7. Future work 54

References.. 55

1. Introduction

The term polygonal fault system (PFS) refers to systems of layer-bound, interconnected extensional faults with a wide range of different strike orientations. The intersecting faults in a PFS form a horizontal polygonal pattern that can be observed in map view of e.g., mapped faults or in seismic data sets (Cartwright, 2003). PFSs are found within very fine-grained sedimentary sequences, in lithologies ranging from smectitic claystones to biogenic sediments like oozes and chalks (Cartwright & Dewhurst, 1998). Sequences hosting PFSs are commonly found in non-tectonic and passive depositional settings, e.g., sedimentary basins at passive margins and intra-cratonic basins (Goulty, 2008).

Research of polygonal fault systems began when in the late 1980s when they were recognized as soft-sediment deformation features. Some of the earliest research on this topic was done by Henriet et al. (1989, 1991), using 2D seismic data from the Belgian offshore and on Eocene-Oligocene clay outcrops in Belgian quarries. They suggested overpressure caused by density inversion as the cause of the deformation. Higgs and McClay (1993) researched an upslope facing polygonal fault system in the North Sea basin. They interpreted this system as the result of gravitational collapse, where the extension of the faulted sequence was accommodated by under-compressed sediments downslope.

With the adoption of 3D seismic, more detailed mapping of PFSs became possible. In 1996 measurements done by Cartwright and Lonergan (1996) revealed almost uniform extensional strain in a PFS located in the North Sea. Based on these measurements and the apparent lack of compressional features to compensate for the extension of the PFS, Cartwright and Lonergan (1996) suggested that a process of volumetric contraction of the host sequence was the cause of faulting and extension. Later Cartwright and Dewhurst (1998) suggested the process of syneresis, a spontaneous process that can expel pore fluids and causes contraction in gel-like substances containing very fine particles, as a possible process that could cause contraction in sequences of very fine-grained sediments. In a response to the suggested syneresis contraction process, Goulty (2001) suggested that the growth of polygonal faults could occur under normal sedimentary compaction load if the fine-grained sequences exhibited a very low coefficient of friction.

With several different processes suggested as possible alternatives for the formation of polygonal fault systems, there are several ways to interpret the polygonal fault systems present in the northern North Sea basin, the study area for this thesis.

The aim of this thesis is to investigate the clay mineralogy and the presence of biogenic silica in the fine-grained sequences.

As far as we're aware, there have not been any studies specifically investigating the influence clay mineralogy and biogenic sediments like biogenic silica might have on the formation of polygonal faults. The clay mineralogy is of interest to investigate, as the transformation of smectite to illite during burial results in an increase in mineral density, reduction of porosity, and the release of excess water (Hermanrud & Undertun, 2019). This process is therefore quite interesting to attempt to correlate with the presence of polygonal faults. Biogenic silica is another mineralogical factor that would be interesting to correlate to the presence of polygonal fault systems. This biogenic sediment is formed from the skeletal remains of some marine microorganisms like e.g., diatoms. At a given depth, the amorphous biogenic silica (Opal-A) will begin to transform from Opal-A to Opal-CT (Thyberg, 1999). This process weakens the silicious microfossils, causing them to collapse. This results in a reduction in porosity, and releases pore water previously stored in the pores formed by these microfossils. Because of this it is worth investigating if this process can be related to the formation of polygonal faults.

This study will investigate both the clay mineralogy and the presence of biogenic silica in the fine-grained mudstone sequences in the northern North Sea basin. This will be done using mineralogy data gathered from samples taken from wells in the North Sea basin. This data will then be used to compare mineralogy vertically in each well, and laterally across different wells.

Wireline well logs will also be used to determine the bulk density of the sequences. This will allow us to estimate the porosity of the sedimentary sequences, which will help identify any abrupt changes in density and porosity caused by the presence of biogenic silica. The gamma ray well logs can also aid in identify any changes in lithology.

The primary focus of this thesis will be to try and uncover any evidence that either the smectite/illite transformation or the Opal-A to Opal-CT transformation can be correlated to the presence of polygonal fault systems.

2. Geological and theoretical background

2.1 Geological history and setting

2.1.1 The Pre-Cenozoic

The first of the two most significant geological developments in the area of the North Sea during the Pre-Cenozoic were the formation of the Caledonian Orogeny during the Ordovician to Early Devonian periods. This orogeny was the result of the collision and merger of the continents Laurenta and Baltica. The collision and merger of these two continents occurred along what is today known as the Appallchian mountain range in north-eastern North America, and the Scottish-Norwegian Caledonian foldbelt. During the Devonian and Carboniferous, the Caledonian Orogeny went through the process of orogenic collapse. (Ziegler, 1975; Coward, 2003).

2.2 Polygonal fault systems

2.2.1 Description of polygonal fault systems

Polygonal fault systems (PFSs) are a type of non-tectonic, interconnected faults which are found in fine-grained sedimentary lithologies. These fault systems are primarily observed in passive depositional settings, most commonly in sedimentary basins, using seismic surveys.

A polygonal fault system is defined as a network of partially and/or fully interconnected extensional faults with a wide range of different strike orientations. When observed in a horizontal time or depth slice in seismic data using variance maps, the interconnected faults form a repeating polygonal pattern.

These fault systems are usually restricted to a host sedimentary sequence, or a set of sequences composed primarily of fine-grained sediments, e.g., different types of clays and chalks. The range of strike orientations in PFS can be influenced by local stress regimes during the formation/growth of the fault system, causing certain strike orientations to become more preferential. In such cases, PFS might appear similar to and be hard to differentiate from other types of sequence-bound faulting, e.g., slump faults and detached growth faults (Cartwright, 2003).

Polygonal fault systems have been discovered in sedimentary basins worldwide (Fig. AAA). They are primarily observed in slope settings at continental margins, which hosts more than

90% of the observed polygonal fault systems. The remaining PFS have been observed at basin floors, intracratonic basins and foreland basins (Cartwright 2011).

Polygonal fault systems are usually widely developed and can cover large areas of the basin. They commonly cover areas greater than 50,000 km2 (Goulty 2008), with some of the larger PFS covering areas in the range of millions of square kilometers. An example of this is found at the Eromanga basin in Eastern Australia, which hosts a PFS that cover an area greater than 2,000,000 km2 (Cartwright 2011).

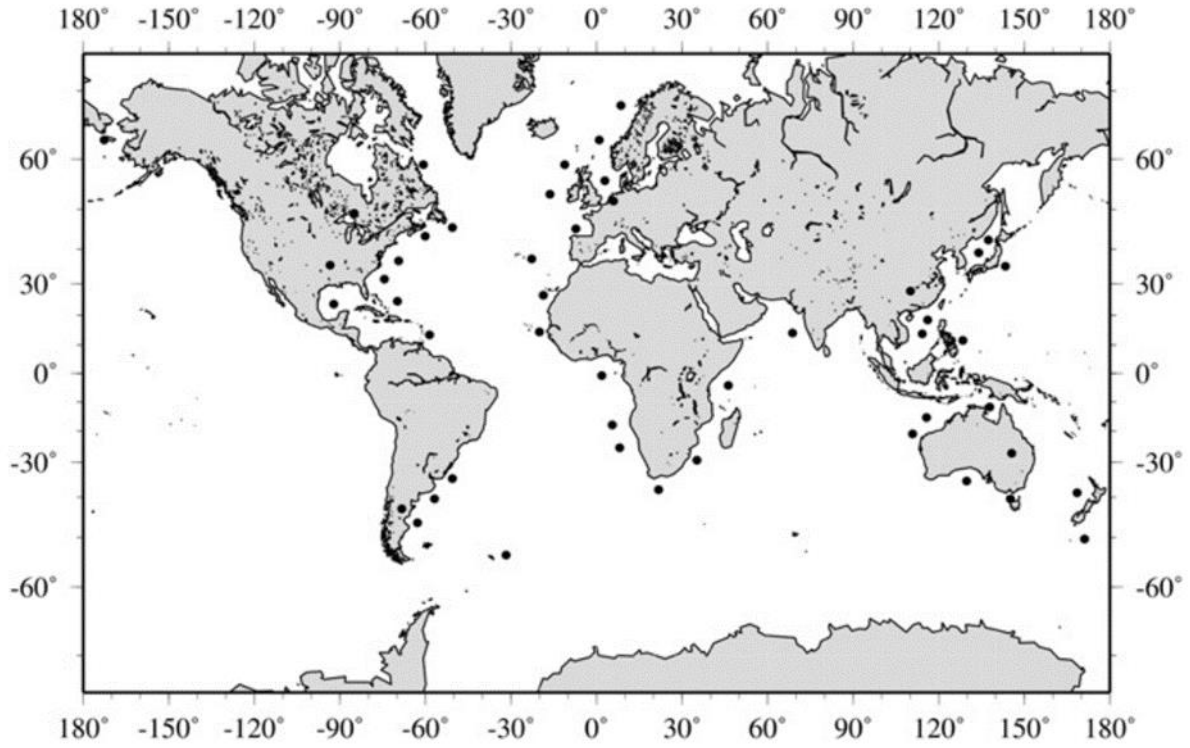

Figure 2-AAA: Map overview of sedimentary basins known to host polygonal fault systems (Cartwright, 2011).

In the passive depositional settings where PFS are observed, the extensional faulting is not the result of tectonic extension. In this setting, the vertical stresses caused by burial and compaction of sediments would be the primary force working on the sedimentary units. Since there is no tectonic extension of the basin, the horizontal extension of a sequence hosting PFS must be accompanied by a horizontal contraction (or general contraction/shrinking) of the faulted unit (Goulty, 2008).

The PFS are hosted in fine-grained sedimentary sequences with a clay fraction greater than 70%, with lithologies ranging from claystones to chalks (Goulty 2008). Polygonal faults often form in different tiers within the host sequence (Fig. BBB), where the majority of faults within a tier is confined to that tier. Larger faults within host sequence can intersect several tiers, forming interconnections between the different tiers. The boundaries of tiers often correspond with stratigraphic units, suggesting that the formation of different tiers is linked to changes in lithology (Cartwright, 2003).

The faults in a typical polygonal fault system are spread apart with a spacing between the faults ranging from 100 m to 1000 m. The faults are either planar or mildly listric and have dips ranging from 30° to 70° (Fig. BBB). Fault throw is usually no larger than 100 m (Goulty 2008).

Fault growth/fault throw in a PFS is very slow compared to tectonic faults. Measurements performed by King and Cartwright (2020) on the fault throw rates of a polygonal fault system in the Vøring basin showed that the faults in this PFS had a throw rate between 1.4 and 10.9 m/Ma, with the median rate of the faults being 5.6 m/Ma (Fig. CCC). When compared to other tectonic and gravity-driven fault systems, polygonal fault throw rates can be up to three orders of magnitude slower (Fig. CCC) (King and Cartwright, 2020).

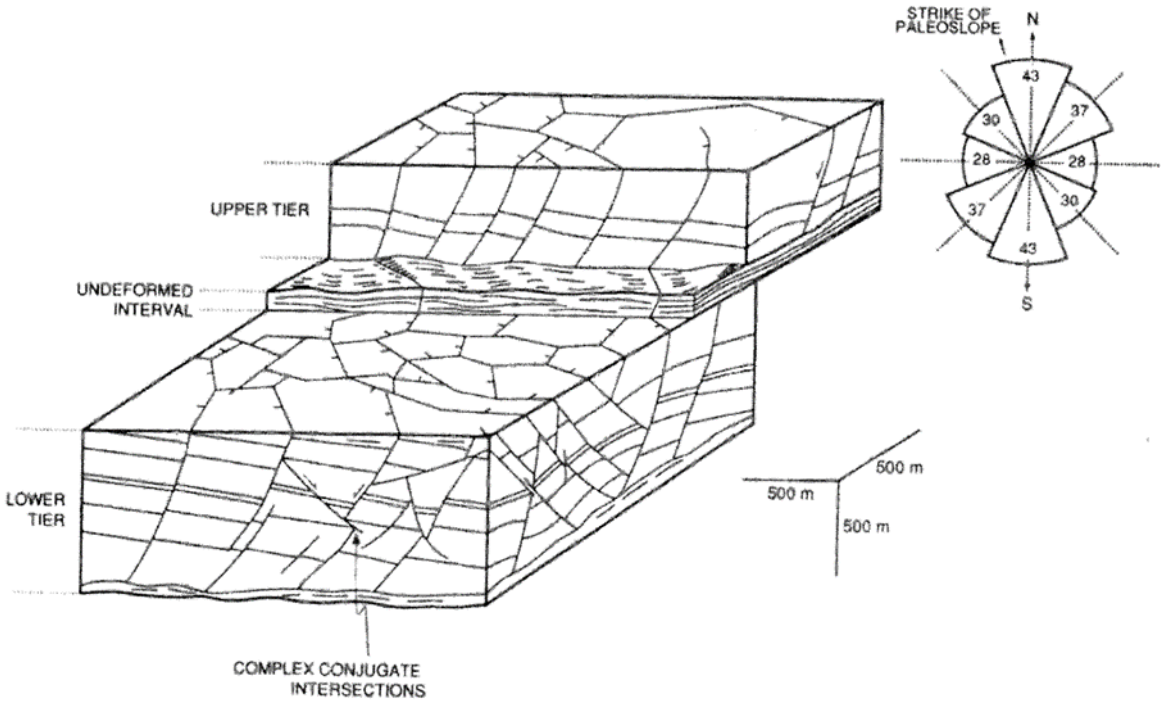

Figure 2-BBB: Example of a polygonal fault system separated into two tiers. The horizontal slices show an example of the polygonal pattern of PFS. The rose diagram shows a strike orientation preference towards N-NE and S-SW (Cartwright, 2003).

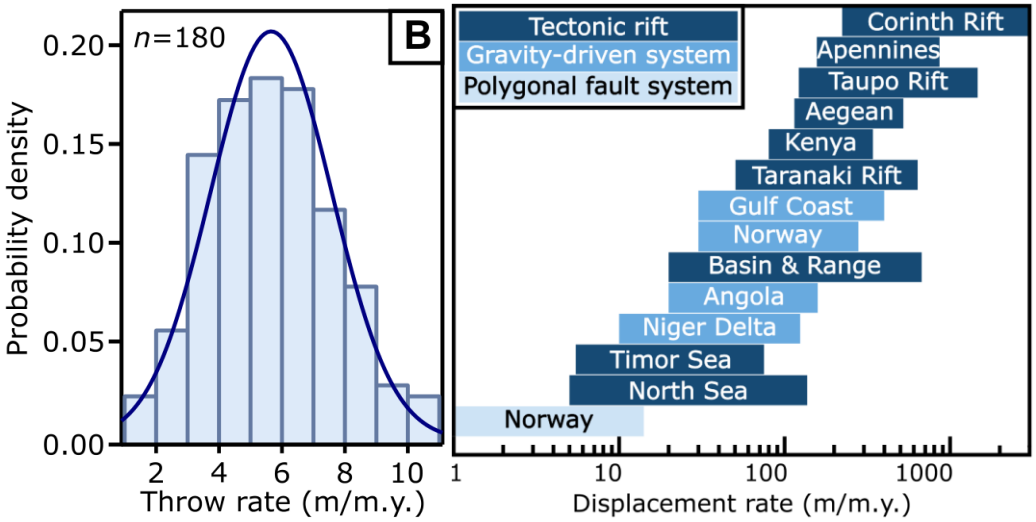

Figure 2-CCC: Fault throw rate of faults in the Vøring basin (left), throw rates of polygonal fault systems compared with tectonic and gravity-driven systems (King and Cartwrignt, 2020).

2.2.2 Suggested formation mechanisms of polygonal fault systems

Gravitational sliding

This model was proposed in Higgs & McClay (1993). It suggests that polygonal faults are the result of failure in a sedimentary unit deposited in a slope setting. Gravity causes the unit to slide downslope, breaking it up and gives rise to the faults. The basal detachment of the sliding sedimentary unit forms the boundary between the faulted unit and the undeformed sediments below (Cartwright, 2003).

This model is not without its limitations. It predicts that the faults would be strongly aligned parallel to the direction of the slide. This is not the case with most polygonal fault systems, where fault strike orientations are widely varied. The model would also be limited to slope settings such as the continental margin (Cartwright, 2003). Although this is the most common setting for polygonal faults to be found in, polygonal faults are also found in settings without any slope, such as the abyssal basin floor (Cartwright, 2011).

Due to these limitations, this model is not considered to be a viable general model to explain the formation of polygonal faults. It is however likely that gravitational stresses influence the formation of the faults in slope settings. In this setting, fault plane orientations would show a preference dipping towards and away from the direction of the slope (Cartwright, 2003). An example of this can be seen in figure 2, where fault strike orientations show a preference dipping towards north-northeast and south-southwest.

Density inversion

This model was proposed in Henriet et al. (1989) and is dependent upon the formation of a reverse density gradient during burial of the sediments. This can occur when a clay unit becomes sealed during burial, preventing dewatering of the sealed unit. The higher content of pore fluid in the sealed unit results in a lower density. A unit of denser clay is then deposited above the sealed unit, forming a reverse density gradient (Fig. DDD) (Cartwright, 2003).

Due to Rayleigh-Taylor instability caused by the difference in density between the two units, they deform into synclinal and anticlinal density inversion folds. With increasing compaction, the deformation strain and fluid pressure increased, eventually causing the formation of faults. Pore fluids escape along the faults, decreasing the pore pressure in the sealed unit (Fig. 4). The process continues until the sealed unit is compacted and in equilibrium with the sedimentary units above (Cartwright, 2003).

A polygonal fault system found in seismic data from Lake Hope at the Eromanga basin in Australia shows a clear pattern of synclines and anticlines, which is cited as evidence in support for the density inversion model. However, many polygonal fault systems do not show any signs of density inversion folds. These fault systems would be difficult to explain with this model (Cartwright, 2003).

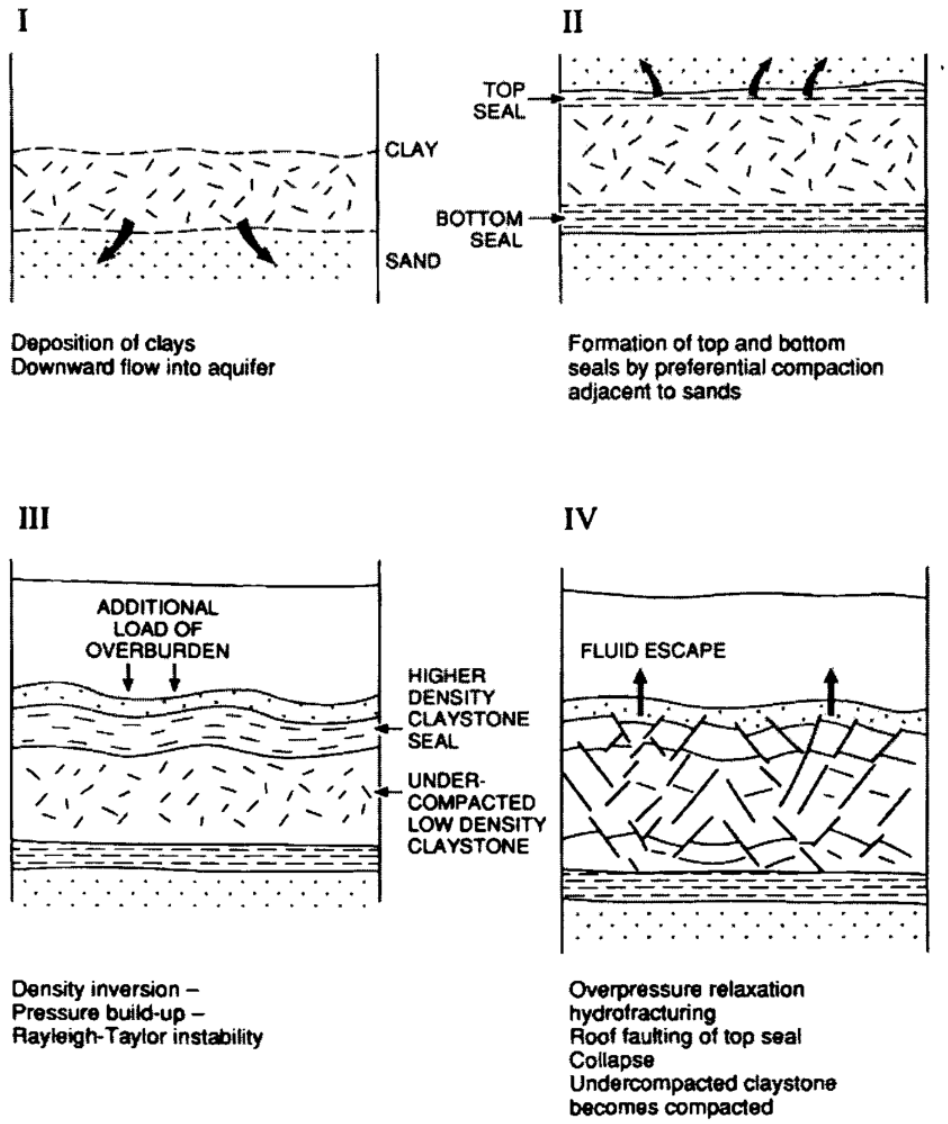

Figure 2-DDD: Four-stage model showing the formation of a reverse density gradient, density inversion folds and failure leading to fluid escape and faulting (Cartwright, 2003)

Syneresis

This model is based on the idea that a sedimentary unit can contract, forming polygonal faults in the process. Syneresis is a process where a material undergoes spontaneous contraction, without evaporation being involved. This is a process that only occurs in gels. If it is to be used as an explanation for the formation of polygonal faults, it must be assumed that the sedimentary unit was in a gel-like state during deformation (Cartwright, 2003).

A gel is defined as a framework of very small colloidal particles. Clay-sized particles are small enough to fit this definition, and clay samples show that the fine-grained sediments found in

polygonal fault host sequences are small enough for these sedimentary units to potentially be in a gel-like state (Cartwright, 2003).

It is proposed that when a sedimentary unit in a gel-like state undergoes syneresis, the clay particles in the gel framework move closer together and expels excess pore fluid from the framework. This causes the sedimentary unit to contract, forming the polygonal faults. The expelled pore water needs to be removed from the unit for it to contract, meaning a fluid escape pathway is necessary. In this case, fluid escape along the fault planes is a likely candidate, especially during fault slip events (Cartwright, 2003).

The continued removal of pore fluids along faults could help maintain the syneresis process and the growth of the polygonal faults. Some evidence exists supporting the claim of fluid flow along fault planes. Displaces microfossils have been found in the fault gouge of polygonal faults (Cartwright, 2003), and fluid escape features has been observed in the overburden above polygonal fault systems (Goulty, 2008).

The supposed syneresis process in sedimentary units is not well understood, particularly what its trigger mechanisms are. Osmosis has been proposed as a mechanism in smectite-rich clays, where syneresis is induced by osmotic effects resulting from changes in salinity and ionic concentrations in the sedimentary unit (Cartwright, 2003).

This model does have some weaknesses. Polygonal faults have been found in freshwater settings, showing that saline pore fluid from seawater is not necessary. This weakens the theory supposing osmosis as the trigger mechanism for syneresis. The fault growth of polygonal faults is thought to be active over millions of years. This causes problems for the syneresis model, as all known syneresis processes are much faster than this and would be almost instantaneous when viewed on a geological timescale (Goulty, 2008).

Low coefficients of residual friction

In this model, vertical stress from gravitational loading (K_0) can lead to shear failure in some sediments without the help of additional stresses or overpressure. This can occur in sediments/lithologies which have low coefficients of residual friction (μ_r) (Goulty, 2008).

This coefficient determines the residual shear strength between two fault planes. A low μ_r therefore reduces the stresses necessary to cause a fault slip. μ_r is known to decrease with increasing clay fractions, meaning that the clay-rich lithologies hosting polygonal faults are

likely to have weak residual shear strength between the faults. If weak enough, stresses from gravitational loading alone can be enough to cause fault slips (Goulty, 2008).

This model relies of the assumption that the faults are already present and cannot be used to explain the initial formation of the faults. It can however explain the continued growth of the faults with a very simple model. It also relies on the values of μ_r being low, and K_0 high enough to overcome residual shear strength. Knowledge of the values of K_0 in polygonal fault systems are however lacking. This makes it hard to test the validity of this model, in both *in situ* studies and in laboratory experiments (Goulty, 2008).

Diagenetically-induced shear failure

This model proposes that shear failure in a sedimentary unit is caused by diagenetic changes in the sediments. It is based on laboratory experiments performed by Shin et al. (2008), using salt and small glass grains as analogues to sediments. These experiments showed that under compression, the ratio of horizontal to vertical effective stresses would decrease from values between 0.53 and 0.68 to values below 0.40 during the salt dissolution diagenesis. This change in stresses caused shear failure in the sediments (Cartwright, 2011).

Besides the dissolution of grains, other diagenetic changes can also affect the stresses in sediments. For instance, a fine-grained silty clay with a 70% clay fraction would be strongly affected by any diagenetic changes that weakened the interactions between the clay particles. This could strongly alter how stresses are distributed within the sediments, possibly causing the clay grains to contract, slip and realign. A chain reaction of such realignments could be the nucleation/initiation of a fault. Changes in the interaction between particles can therefore result in macro-scale share failure in the sediments (Cartwright, 2011).

Although diagenetic changes can affect many types of sediments, shear strain failure of this type and size likely only occurs in sediments that exhibit post-peak strength softening. This is a property typical of clay-rich sediments with low residual friction, which also happens to be the type of lithology polygonal faults are typically hosted in (Cartwright, 2011).

A strong argument in favor of this model is the large lateral scale some polygonal faults can cover. Diagenetic process in similar sediments should be the same at similar depths. If diagenesis is the formation mechanism, it can explain how polygonal fault systems can form in and cover large areas (Cartwright, 2011).

2.3 Opal-A to Opal-CT transformation

Opal-A refers to the amorphous silica that makes up the skeletons of some microorganisms like diatoms and radiolarians. This amorphous silica becomes increasingly soluble with increasing temperatures during burial. The Opal-A to Opal-CT transformation refers to a diagenetic process based on a solution-redeposition mechanism, in which Opal-A is dissolved and microcrystalline cristobalite and tridymite is redeposited from the solution. Given enough time or preferably higher temperatures, Opal-CT would be diagenetically transformed further into chert (Kastner et al., 1977).

When sediments rich on Opal-A from biogenic silica undergoes the transformation to Opal-CT, the weakened skeletal remains of diatoms and other silicious microfossils are more likely to be crushed during burial. When crushed, the pore spaces these skeletons provided is reduced, and the pore fluids within expelled. Sediments containing biogenic silica will exhibit an abrupt reduction in porosity and increase in density at the depth where the transformation occurs. This change might be visible as a reflector in seismic surveys, as an reflection that is mostly horizontal and that crosscuts other stratigraphy (Hermanrud & Undertun, 2019)

3. Data and methods

This chapter gives an overview of the seismic data, well log data, and mineralogy data used in this thesis. It also explains any methods used to process the data.

3.1 Seismic data

A 3D seismic data set covering the study area in the northern North Sea was used to in this thesis. This dataset (NVG Final_Ki-PreSDM_Z_Fullstack_5.3.1) is a Kirchhoff Pre-Stack Depth Migrated 3D seismic volume of the North Viking Graben. It was provided by the multinational geoscience technology service company CGG through the University of Bergen. The seismic volume has a crossline interval of 12.5 m, and an inline interval of 18.75 m.

It fully covers the North Sea quadrants numbered 34, 35, and 30, with mostly full coverage of 35. It has partial coverage of the quadrants 33, 36, 29, 32, 25 and 26 (see Figure 3-1).

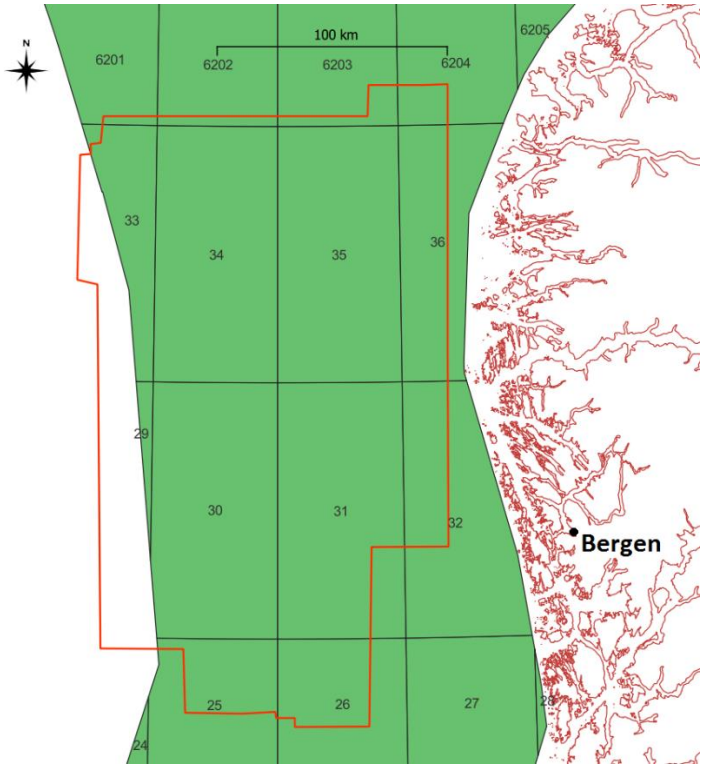

Figure 3-1: The location of the 3D seismic survey outlined in red, showing which North Sea quadrants are covered by the survey. The outline of the Norwegian coast is included to show the scale and location of the seismic survey.

The 3D seismic survey was viewed using the Petrel 2019 E&P (exploration and production) software platform, developed by Schlumberger Limited. This software has a lot of use cases, from e.g., viewing and interpreting seismic reflections, to displaying wells in seismic lines and map view, reading well logs, and making reservoir models.

In the making of this thesis, petrel was used extensively to view and do measurements on seismic lines, explore the seismic near wells with relevant well log or mineralogy data, and create figures used in the thesis. Such figures include map views, overview figures of stratigraphic sequences viewed in seismic lines, figures of wells showing at which depths different mineralogy samples was collected, and well logs showing e.g., gamma ray and bulk density.

Previous work done by a former master student at the Department of Earth Science at the University of Bergen, Amalie Sande Rødde, was imported over and used in this making of this thesis. For her thesis, *Polygonal faults in the northern North Sea*, she interpreted the Cenozoic Sequence Stratigraphy (CSS) of the study area in the northern North Sea (Jordt et al., 1995) using the seismic interpretation tools in the Petrel software.

Although she used the same seismic data set as was used for this thesis, hers were time-migrated instead of the depth-migrated. To make use of these interpreted sequence horizons, we used a built-in of petrel to make a velocity model based on the "velocity cube" of the seismic survey, a dataset containing the seismic velocities at all points of the seismic volume. Using the velocity model, the interpreted horizons were translated from the Two-way traveltime (TWT) based time-migrated seismic volume to the true vertical depth (TVD) based depth-migrated seismic volume.

The Cenozoic sequence stratigraphy is important to recognize as it very useful when working with seismic lines in the North Sea basin. Figure 3-2 shows the age of the different Cenozoic sequences and which epochs they are associated with.

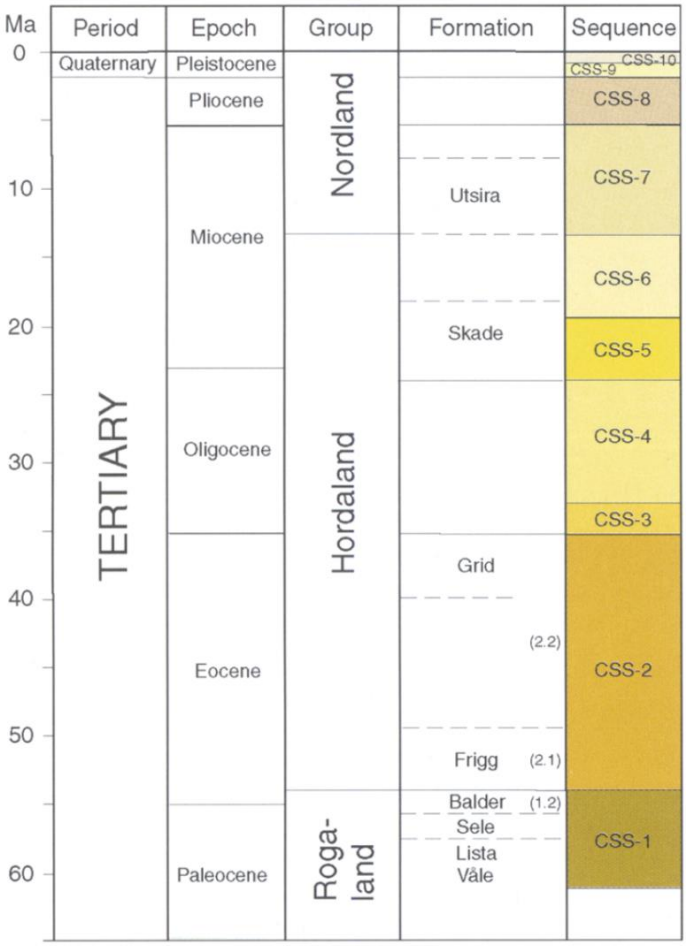

Figure 3-2: Cenozoic seismic stratigraphic framework from Faleide (2002), in which this figure was credited to be based on work done by Jordt et al. (1995, 2000). The framework shows what sedimentary groups and geological epochs each CSS is associated with.

The CSS-1 sequence was deposited during the Late Paleocene and earliest Eocene. The top of CSS-1 corresponds top of the Rogaland sedimentary group (Top Rogaland) and the top of the Balder tuffs. The CSS-2 sequence is of Eocene age, as was deposited from the Early Eocene to the end of the Eocene Top CSS-2 corresponds to the transition to the Oligocene, and is also associated with a hiatus, especially at the flanks of the basin. The CSS-3 sequence was deposited during a short period in the Early Oligocene. This sequence onlaps onto the flanks of the basin margin. The top of CSS-3 represents the mid-Early Oligocene. The sequence CSS-4 was deposited during the Oligocene, with the top of the sequence representing the end of the Oligocene. The sequences CSS-5, CSS-6 and CSS-7 represents the Miocene sequences, with the top of CSS-6 being accosiated with the top of the Hordaland sedimentary group. (Faleide, 2002).

Of the Miocene sequences, CSS-6 and its top boundary is of most interest. This bouandry (Top CSS-6 or Top Hordaland) represents the shallowest sequence in which polygonal fault systems can be observed in the study area. The regional seismic line (Figure 3-3) made by Faleide (2002) shows how the different sequences are typically deposited in the norther North Sea basin and can be of aid when trying to identify them in seismic lines.

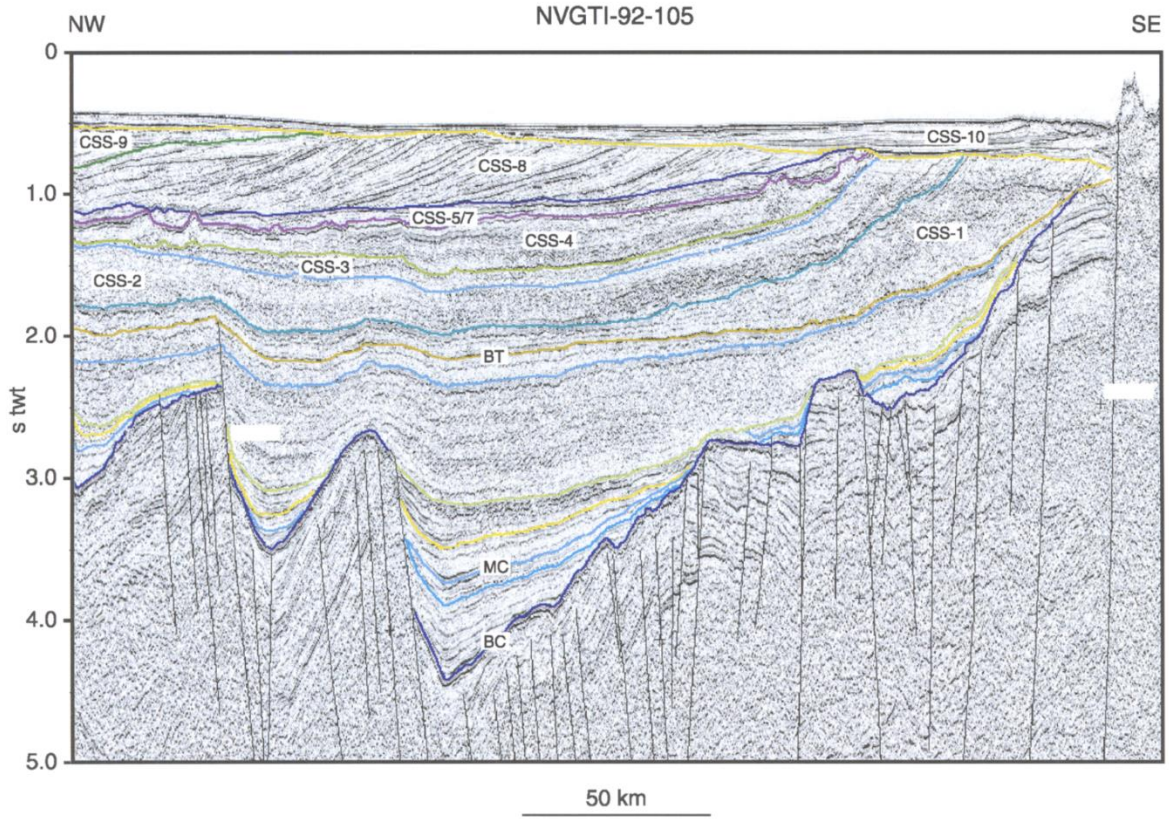

Figure 3-3: Regional seismic line with interpretation showing the sequences CSS-1 to CSS-10 and the horizons separating the sequrences (Faleide, 2002) The horizon BT (Base Tertiary) is referred to as Base Paleocene or Top CSS-0 in this thesis.

3.2 Mineralogy data

The clay mineralogy data used in this thesis is based on previous work done by Dr. Yngve Rundberg in his thesis "*Tertiary sedimentary history and basin evolution of the Norwegian North Sea between 60°- 62° N – an integrated approach".* Ten data sheets in the appendix of Rundbergs thesis contains measurements of clay minerals in samples taken at intervals in ten different wells. Seven of these wells and associated mineralogy data was used in this master's thesis (Rundberg, 1991).

X-ray diffraction analysis were used to determine the clay mineralogy. It is explained in Rundberg (1991) that a <6µm fraction of the samples were used for the analysis of clay minerals. This fraction was chosen instead of the <2µm conventional bouandry between clay sizes and silt sizes. The reason for this is to allow through detrital clay minerals which can have different clay sizes, some that would not pass through the <2µm fraction. As such, using the <6µm fraction would better represent the bulk of clay minerals in the sample, giving a more accurate measurement of the clay mineralogy. This fraction would also allow significantly more non-clay minerals (e.g., quartz and Opal-CT) to pass through and be recorded as well (Rundberg, 1991).

The data sheets show for each sample at different depths; the estimated percentage of the clay types smectite, illite, kaolinite and chlorite. The measurements of these four clay minerals add up to 100% of the clay content observed in one given sample. The data sheets also show estimated values for some non-clay minerals. See Figure 3-2 for an example of these data charts. The non-clay minerals are presented slightly differently. Rather than being in a separate group like the clay minerals are, the most abundant of the <6µm non-clay minerals (e.g., quartz, feltspat, calcite and Opal-CT) are presented as a percentage of the total amount of <6µm minerals present in each sample (Rundberg, 1991).

The data sheets in Rundberg (1991) does not show the numerical values for each data point but is instead presented in horizontal bar charts. To translate these into numerical values, digital measuring tools were used on scanned photocopies of the data sheets (Figure 3-2). By measuring the length of the bar charts (in pixels), a reasonable estimate of its value could be made. The same method was used to determine the depth of the samples, as depth is shown on the data sheets in intervals of 100 meters. Values determined by this method was rounded to the nearest whole number. A percentage value of e.g., 30.34 would be rounded down to 30. The same rounding was done when determining the depth of each sample.

APPENDIX 4

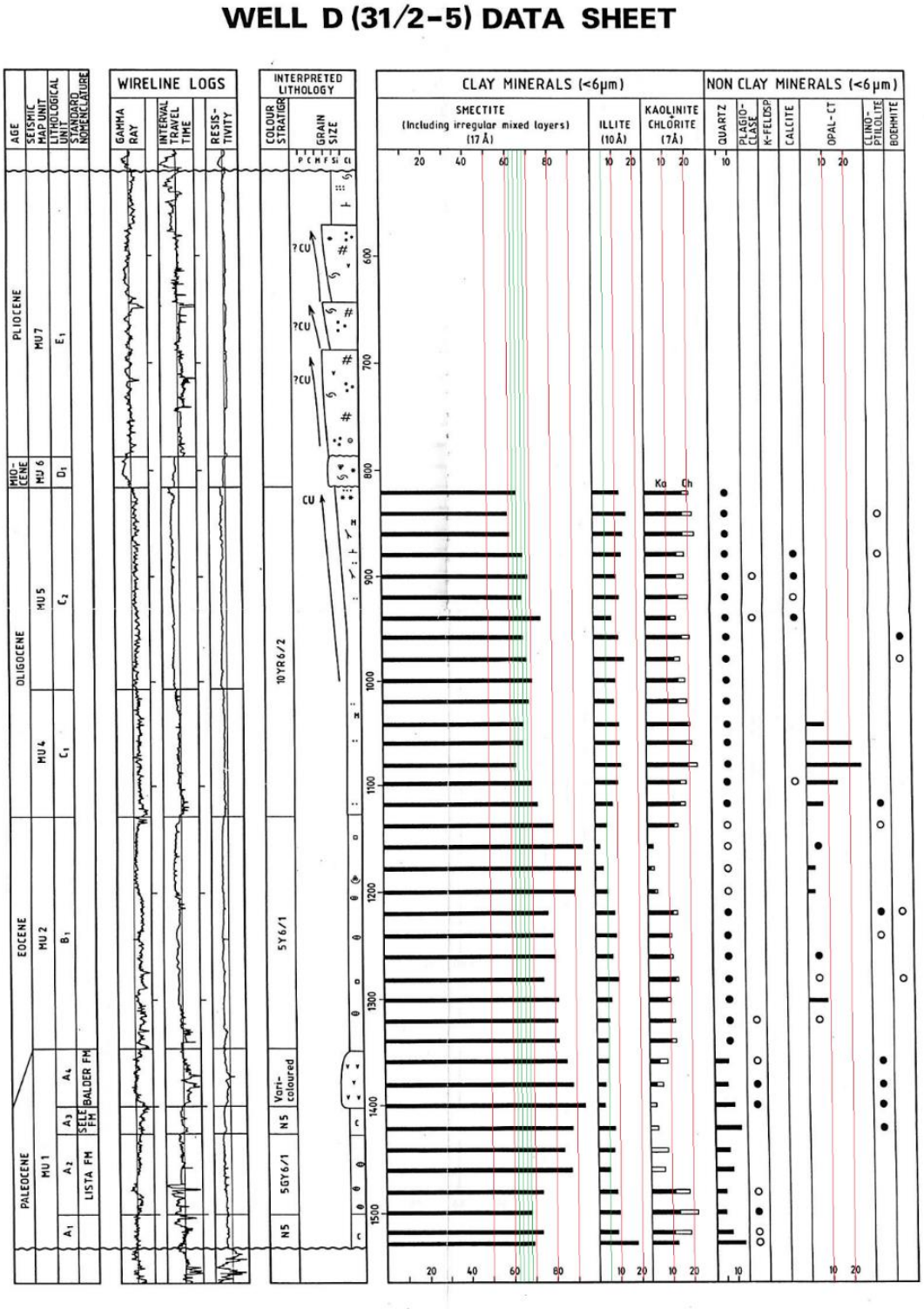

Figure 3-2: Data sheet showing measurements of clay minerals and non-clay minerals found in samples from the well 31/2-5 in the North Sea (Rundberg, 1991). The red and green lines was added to aid in the translation from bar chart to numerical values.

3.2.1 Uncertainties

The mineralogy data translated from the data sheets were for the sake of efficiency rounded down to the nearest whole percentage. A percentage of e.g., 31.3% would be rounded down to 31% Due to this some of the total percentage values of the clay minerals at certain depths might be slightly above or below 100%. This uncertainty is unlikely to have any large impact on the quality of the data. This is because the inherent uncertainty of quantifying different clay minerals in a mix from one another is larger than the uncertainty introduced by the rounding of the measured bar charts. The average error in the quantification of the clay minerals is given in Rundberg (1991) to be around 5% to 10%. The clay mineralogy measurements are meant of give an overview of the bulk clay sedimentology over large depths. It might be anywhere from 20 to 50 meters in between samples depending on the well. The samples are meant to give an overview of the bulk of clay mineralogy through several sedimentary sequences. A small measurement error would not have a large impact on the larger picture in this instance.

3.3 Wells and well logs

Wells are used in this thesis as a source of both mineralogical measurements from samples and wireline measurements from drilling. Figure 4-3 show the location of the wells used in this master's thesis. These wells provided either mineralogy data, well log data (e.g., gamma ray and bulk density), or in some cases both.

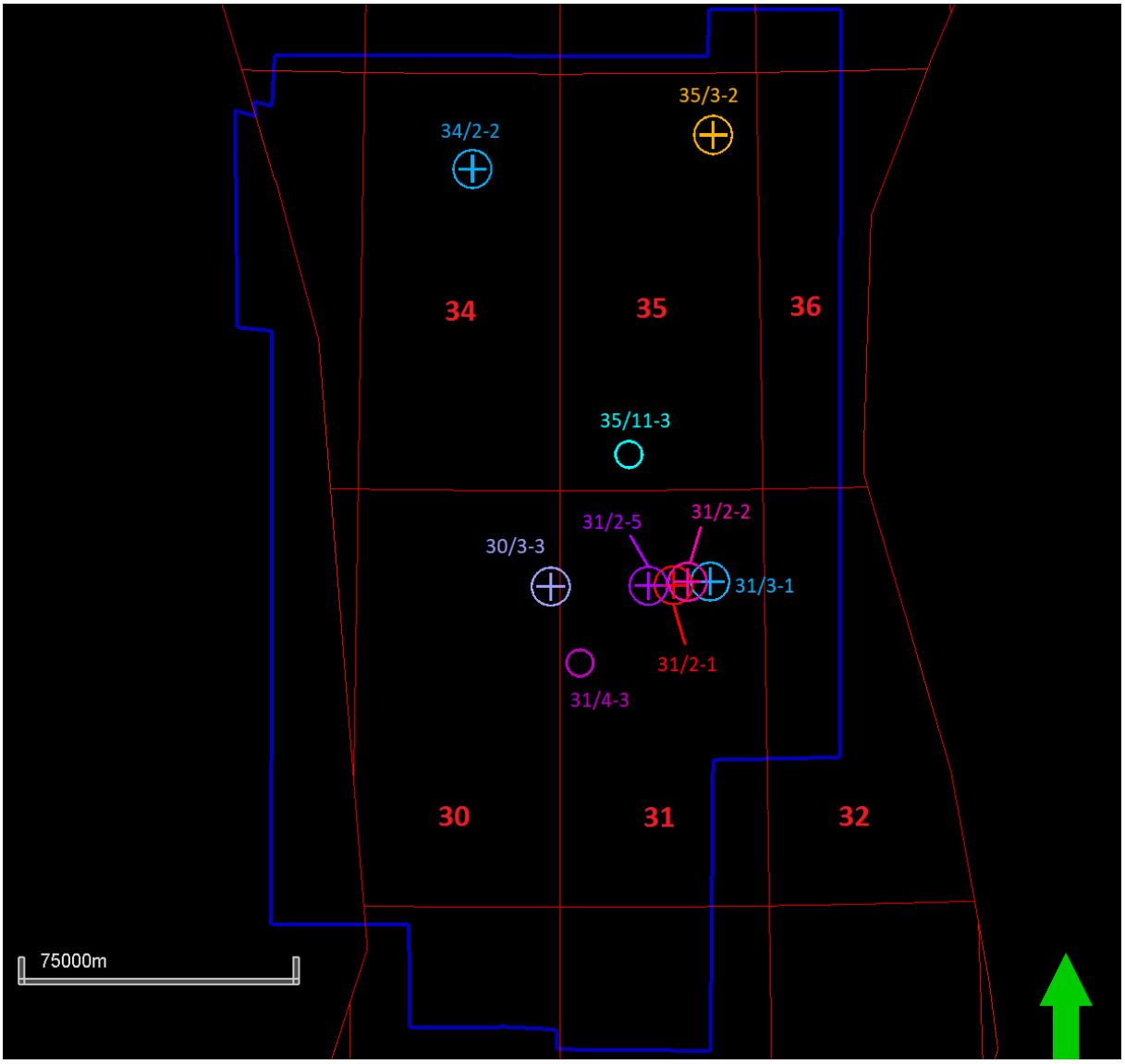

Figure 3-4: Map view showing the outline of the seismic survey, along with the wells used in this master's thesis. The wells with shown as (+) signs are wells with mineralogy data, the ones shown as normal circles are wells with well log data, but no mineralogy data.

The following table (Table 3-1) gives an overview of what type of data each well provided:

Table 3-1: Table showing the different data types that was used from each well.

Well:	Well logs	Clay mineralogy	Opal-CT
30/3-3	X	X	X
31/2-5	X	X	X
31/2-1	X	X	X
31/2-2	X	X	X
31/3-1		X	X
34/2-2		X	
35/3-2		X	X
31/4-3	X		
35/11-3	X		

The well logs used in this master's thesis were downloaded from the Diskos National Data Repository (NDR). Diskos NDR is the Norwegian data repository for petroleum data, a database operated by the Norwegian Petroleum Directorate (NPD) and oil companies present on the Norwegian continental shelf. This database contains data relevant to the petroleum industry, e.g., well logs and seismic data (Norwegian Petroleum Directorate, 2023).

Well logs are measured from the drill floor of the drilling rig that drilled and logged said well. This ls often referred to as rotary kelly bushing. While the kelly bushing is an important piece of drilling equipment found on the drill floor, literature regarding wells, well logs and drilling often refer to *Measured Depth* from the *Rotary Kelly Bushing*. Shortened abbreviations like "MD RKB" or "m RKB" are often used to signify that the depth is not the true vertical depth, but the length the drill cable has traversed from the drill floor.

In a vertical well, this difference can be accounted for by subtracting the height of the kelly bushing over mean sea level. In the case of non-vertical wells, a log of the path the drill head took is needed to calculate the true vertical depth of a given measured depth. When adding well logs to wells in software like e.g., Petrel, this is done automatically assuming the well is set up correctly. The wells used in this master's thesis are older exploration wells and are all basically vertical. Therefore, knowing the height of the kelly bushing is enough to convert these well logs to true vertical depth.

Measurements from some of the well logs are used together with mineralogy data indicating the presence of Opal-CT. The following table (Table 3-2) shows the wells for which well logs were downloaded, and if they can be paired with Opal-CT measurements:

Table 3-2: Overview of wells for which well logs were downloaded from Diskos NDR. The table shows if those logs have measurements of gamma ray and bulk density, and if the well has mineralogy data from Rundberg (1991) regarding the presence of Opal-CT associated with it.

Wells:	**GR and RHO logs?**	**Opal-CT measurements?**
30/3-3	Yes	Yes
31/2-5	Yes	Yes
31/4-3	Yes	No
35/11-3	Yes	No
31/2-1	Yes	Yes
31/2-2	Yes	Yes

The values from the bulk density log will be used to calculate an estimated porosity above and below suspected Opal-A to Opal-CT transformation sites. For this we use this formula:

$$\emptyset = \frac{\rho_b - \rho_w - \rho_{ma}}{-\rho_{ma}}$$

With Ø being porosity, ρ_b being the bulk density from the well logs, ρ_w being the pore fluid density, and ρ_{ma} being the matrix density. For ρ_w, a value of 1 g/cm^3 was chosen, and for ρ_{ma}, a value of 2.72 g/cm^3 was chosen. We chose to use this value for the matrix density as it was used by Hermanrud & Undertun (2019) when doing similar calculations in the northern North Sea.

4. Observations and results

4.1 Mineralogy observations

4.1.1 Clay mineralogy of Well 30/3-3

This well has the greatest amount of usable mineralogy data samples with 44 samples in total. The two uppermost samples show a vastly different clay mineral composition than the rest of the samples (Figure 4-1). These are found in what appear to be prograding clinoforms westwards. Given this and the large amounts of chlorite and low amounts of smectite present, these are very likely samples of the clay content in glacial sediments from the Quaternary, originating from the Norwegian mainland to the east.

Looking at Figure 4.1, we see an increasing fraction of smectite and decreasing fraction of illite in the clay content, starting from the first sample of Miocene age (-800 m), reaching values of around 80 to 90% smectite and less than 10% illite starting near the top of the CSS-2 Eocene sequence at -1660 m, down to a depth below the Top Rogaland Gp. (Top CSS-1) at -2000 m. During this interval we also observe a significant decrease of the kaolinite fraction, and a slight increase in the chlorite fraction. The samples from sequence with visible polygonal faulting, between -979 m and -1500 m, show smectite fractions between 54% and 74% and illite fractions that decrease from 18-15% in the three upper samples, to around 8-12% in the lower samples.

The significant change in seismic facies at Top CSS-3, going from a clear contrast between the peaks and troughs in the sequence above (CSS-4) to almost transparent in the sequence underneath (CSS-3), does not appear to be visible in the mineralogy data. Looking at the sample at -1260 m depth, and the nearby samples above and below it (Figure 4-1), there doesn't seem to be any significantly large changes in clay mineralogy.

From the sample at -2000 m just below Top Paleocene (Top CSS-1) and down to Base Paleocene (Top CSS-0) at -2210, we observe a significant reduction in the smectite fraction of the clay content. This is accompanied by increases to the fractions of illite, kaolinite and especially chlorite. This shows a large change in the clay composition of the Paleocene sequence (CSS-1) compared to the above Eocene sequence (CSS-2)

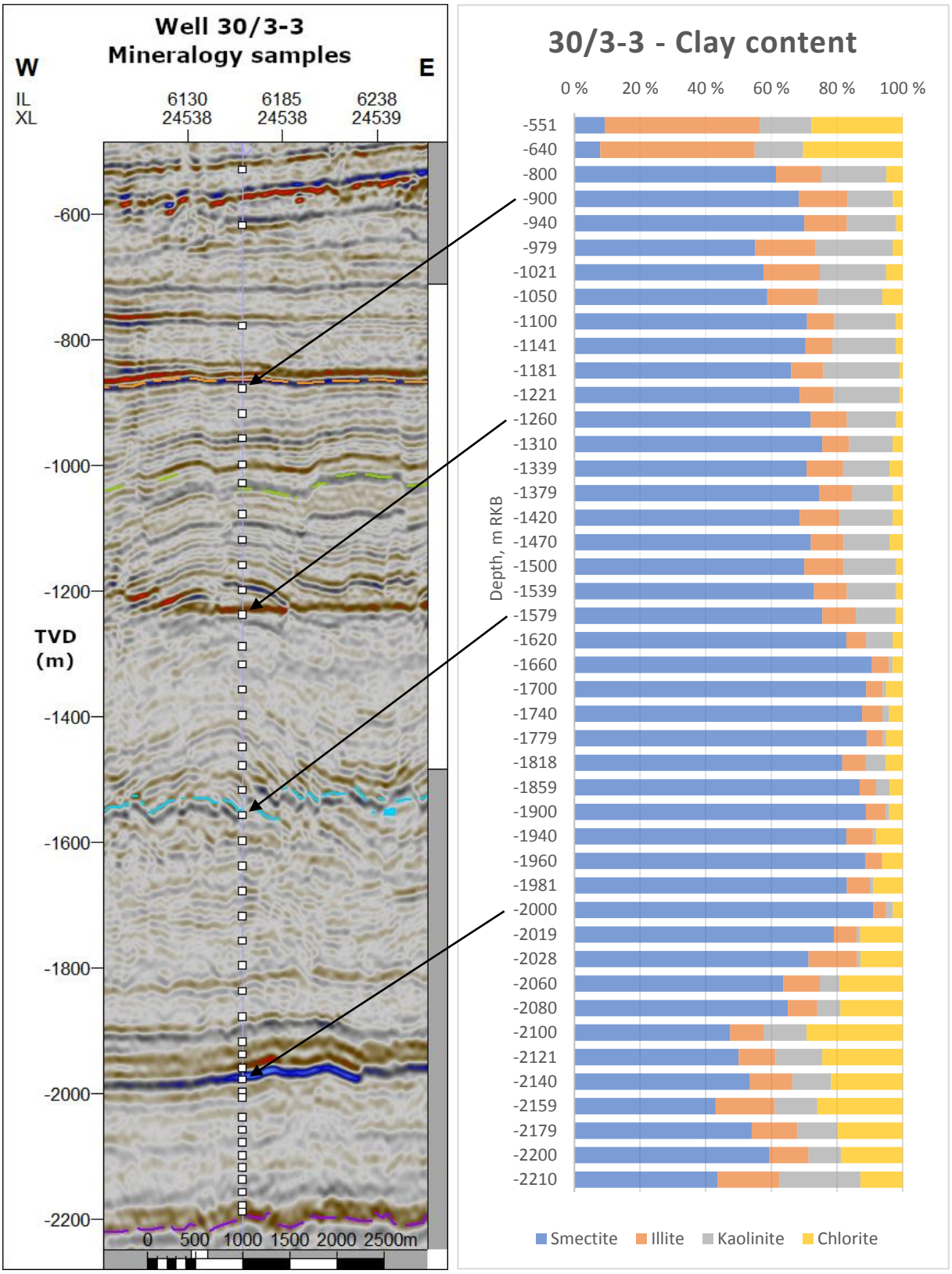

Figure 4-1: Seismic display of well 30/3-3 showing the depth of each sample (left), bar chart displaying clay content of samples (right). The left vertical axis is displayed in True Vertical Depth, the right vertical axis is displayed is measured depth from the well drilling floor (rotary kelly bushing).

To better visualize the changes in the illite fraction compared to the smectite fraction in well 30/3-3, Figure 4-2 displays the fraction of illite content when just smectite and illite are considered. Disregarding the outlier at the stop caused by samples from glacial sediments, we see the illite fraction comparatively to the smectite fraction slightly increase from -900 m to around -1000m. From here the illite fraction of smectite + illite continue to decrease down to around -2000 m. Continuing down, we observe a significant increase in the illite fraction down to Base Paleocene (CSS-0) at -2210 m. This increase observed in the Paleocene sequence (CSS-1) cannot be attributed to the transformation of smectite to illite alone, as the mineralogy data (Figure 4-1) show that this is a very different clay composition, and the total fraction of smectite + illite is lower than in the Eocene (CSS-2) and Oligocene (CSS-3 and CSS-4) sequences.

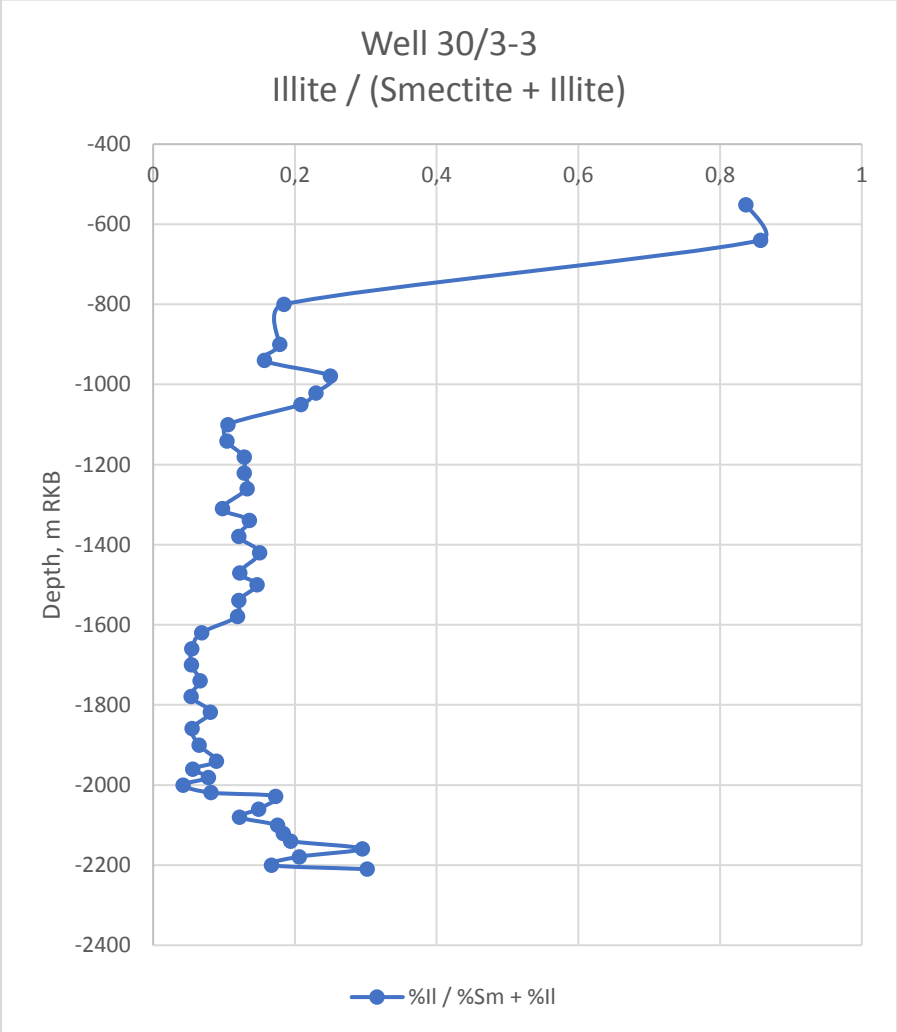

Figure 4-2: Graph displaying changes in the illite fraction of Smectite + Illite in each mineralogy sample from the well 30/3-3. Depth is measured from the well drilling floor (rotary kelly bushing).

4.1.2 Clay mineralogy of Well 31/2-5

The well 31/2-5 is located east of 30/3-3 and is situated at the basin slope. It has 37 samples of mineralogy data in total. Between Top CSS-4 (Top Oligocene) and Top CSS-3 (Top Lower Oligocene), samples taken from -821 m down to -1000 m show modest variations in mineralogy. This trend continues down to the sample near Top CSS-2 (Top Eocene) at -1118 m. The smectite fraction observed in this range is between 61-75%, and illite fraction somewhere between 8-15% (Figure 4-3).

As such, the Upper (CSS-4) and Lower (CSS-3) Oligocene sequences appear to have a similar clay mineralogy, despite the difference is seismic facies between them. This difference is not as prominent here as it is in well 30/3-3 (Figure 4-1), but CSS-3 still has a band of a transparent seismic facies. Prominent polygonal faults are hosted in these two sequences (Figure 4-3).

The upper part of the Eocene sequence (CSS-2), the samples between -1158 m and -1200 m show an high smectite content of 90-90%, which is at greater depths lowered to around 80%. In the upper part of the Paleocene sequence (CSS-1) the samples between -1359 m to -1461 m reveal a high smectite fraction of between 84-94% (Figure 4-3). This is a lot higher than what is observed in well 30/3-3 (Figure 4-1), and this is quite interesting as we can observe two small faults near the well in CSS-1, unlike the CSS-1 sequence at well 30/3-3.

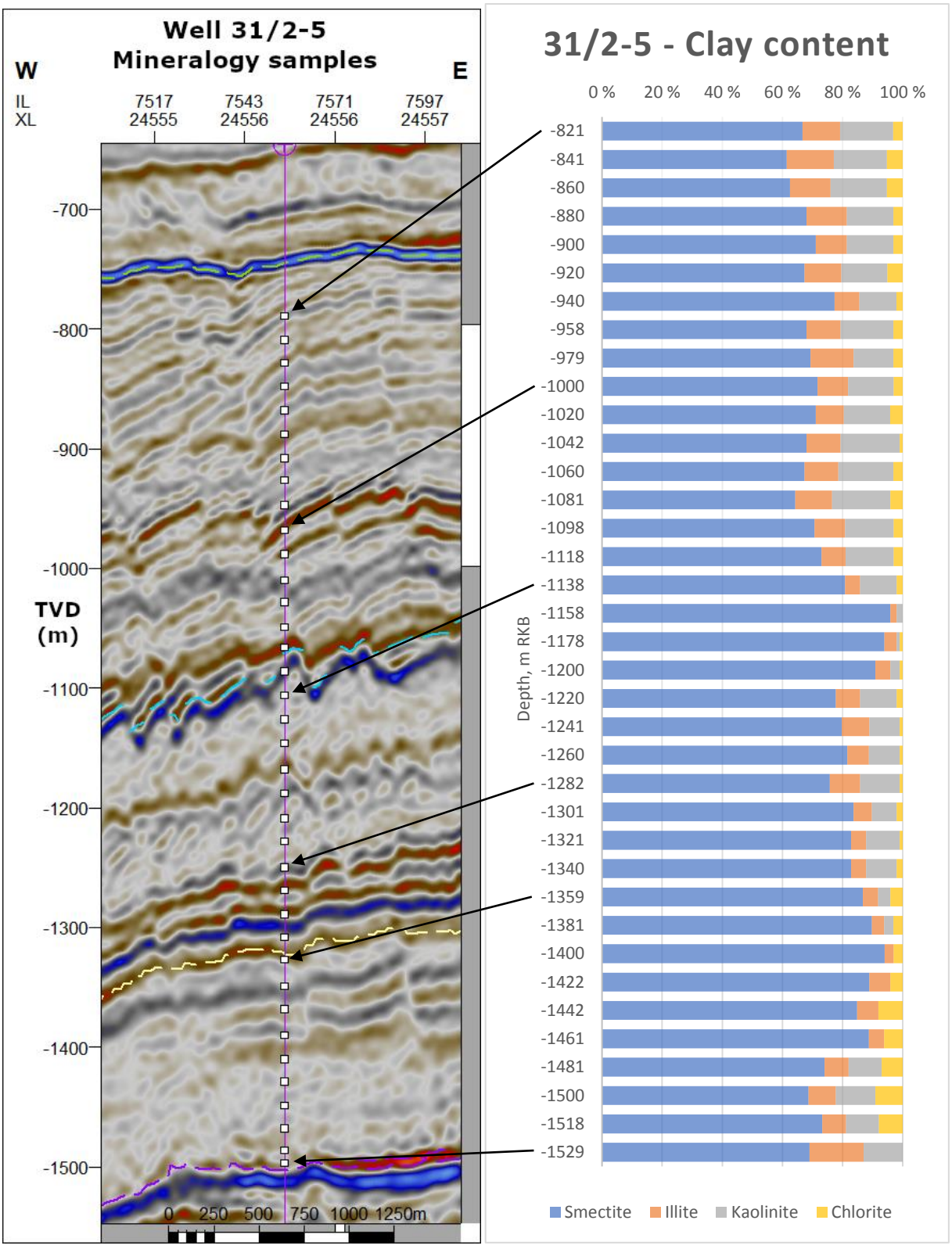

Figure 4-3: Seismic display of well 31/2-5 showing the depth of each sample (left), bar chart displaying clay content of samples (right). The left vertical axis is displayed in True Vertical Depth, the right vertical axis is displayed is measured depth from the well drilling floor (rotary kelly bushing).

Figure 4-4 displays the illite fraction when just smectite and illite are considered. The trend shown from the first sample is a decreasing illite fraction until it reaches the lowest illite fraction at -1158 m depth. From here we see a trend of increasing illite fractions until the sample at -1282 m. Illite fraction then decrease until -1400 m, from where the illite fraction again increase until the last sample at -1529 m.

The samples showing a higher illite to smectite + illite fraction, also show an increase in the fraction of kaolinite and/or smectite. Due to this the increase is not necessarily related to smectite/illite transformation but might be the result of changes in mineralogy between sedimentary sequences.

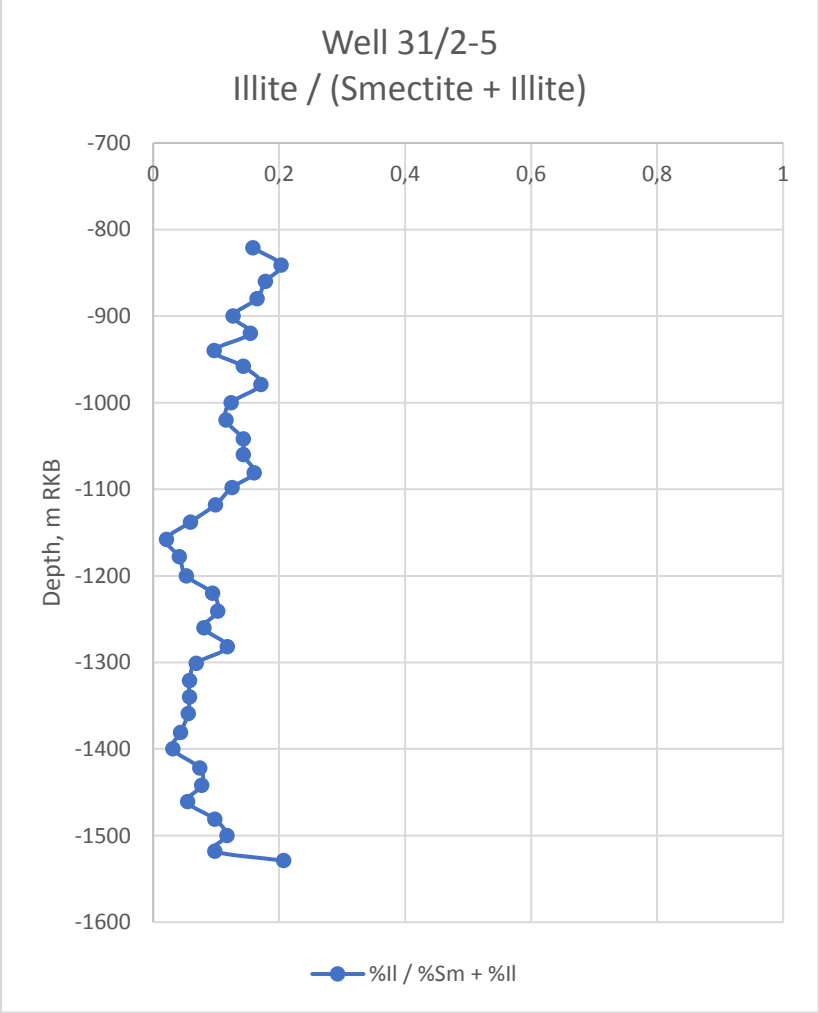

Figure 4-4: Graph displaying changes in the illite fraction of Smectite + Illite in each mineralogy sample from the well 31/2-5. Depth is measured from the well drilling floor (rotary kelly bushing).

4.1.3 Clay mineralogy of well 31/2-1

This well is located east of the well 31/2-5, further up the basin slope. Looking at Figure 4-5, the first two samples are clearly from glacial sediments. The third sample at -640 m is curious. It appears to have too much smectite and too little chlorite to be from glacial sediments yet is seems to be taken from the sequence of prograding coliforms.

In the CSS-4 sequence we see an increase of smectite and reduction of illite from -681 m down to -761 m. The above-mentioned sample at -640 m also seem to bit into this pattern. The remaining samples in CSS-4 from -761 m down to -822 appear to have similar clay content, with a smectite fraction around 69-73% and illite fraction around 9-12% (Figure 4-5). These values are like what was seen in CSS-4 in wells 30/3-3 and 31/2-5.

Underneath CSS-4 is not CSS-3 but some other sedimentary sequence that CSS-3 appear to onlap unto a but further west of this well. The mineralogy of this sequence is markedly different from both CSS-4 above it and CSS-2 below it. Looking at the samples between -840 m to -939 m, we observe a large decrease in the smectite fraction, an increase in the illite fraction and a slight increase in the chlorite fraction (Figure 4-5). The upper part of the Eocene sequence (CSS-2) shows high mounts of smectite, similar to what we see in 30/3-3 (Figure 4-1) and 31/2-5 (Figure 4-3).

It is very interesting to observe that the polygonal faults in CSS-4 seem to disappear around this area where CSS-3 onlaps onto the flank and disappears, and where CSS-4 has changed from being situated on top of CSS-3 to being on top of a different sedimentary sequence.

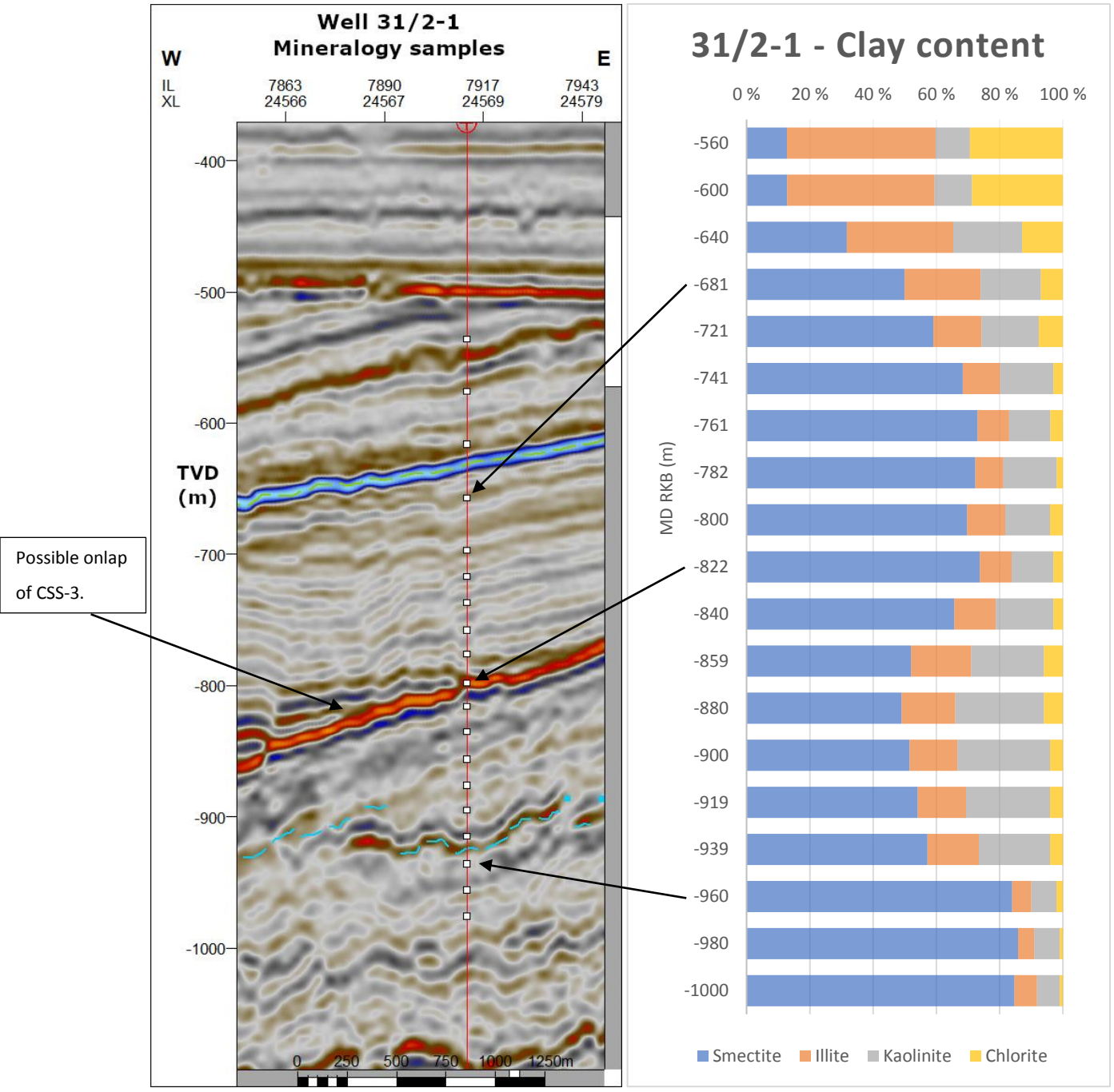

Figure 4-5: Seismic display of well 31/2-1 showing the depth of each sample (left), bar chart displaying clay content of samples (right). The left vertical axis is displayed in True Vertical Depth, the right vertical axis is displayed is measured depth from the well drilling floor (rotary kelly bushing). Near this well we observe the onlap of CSS-3. It might be interpreted to be where the arrow indicates, but there where difficult reflectors to interpret, so the onlap might also be a bit further west.

4.1.4 Clay mineralogy of well 31/2-2

This well is located east of 31/2-1. Looking at Figure 4-7, we see quite high smectite values through the entire well, from the first sample down to -875 we see the sequence under CSS-4 that replaces CSS-3 has a lower fraction of smectite and higher fraction of kaolinite compared to CSS-2 and CSS-1. Polygonal faults do not seem to be present in CSS-4. A single fault in the sequence is visible, although a single fault can not be considered a PFS.

When looking at the illite fraction of (smectite + illite) in this well (Figure 4-6), we see some high values around -850 m at the start of the Eocene sequence (CSS-2), before this is again lowered. We see some spikes of increased illite fraction at -1039 m and -1119 m in the lower parts of CSS-2. From the sample at -1180 m and downwards in the CSS-1 sequence, we see a low fraction of illite in Figure 4-6, due to the fact that the clay fraction of CSS-1 is here around 87-90% (Figure 4-7)

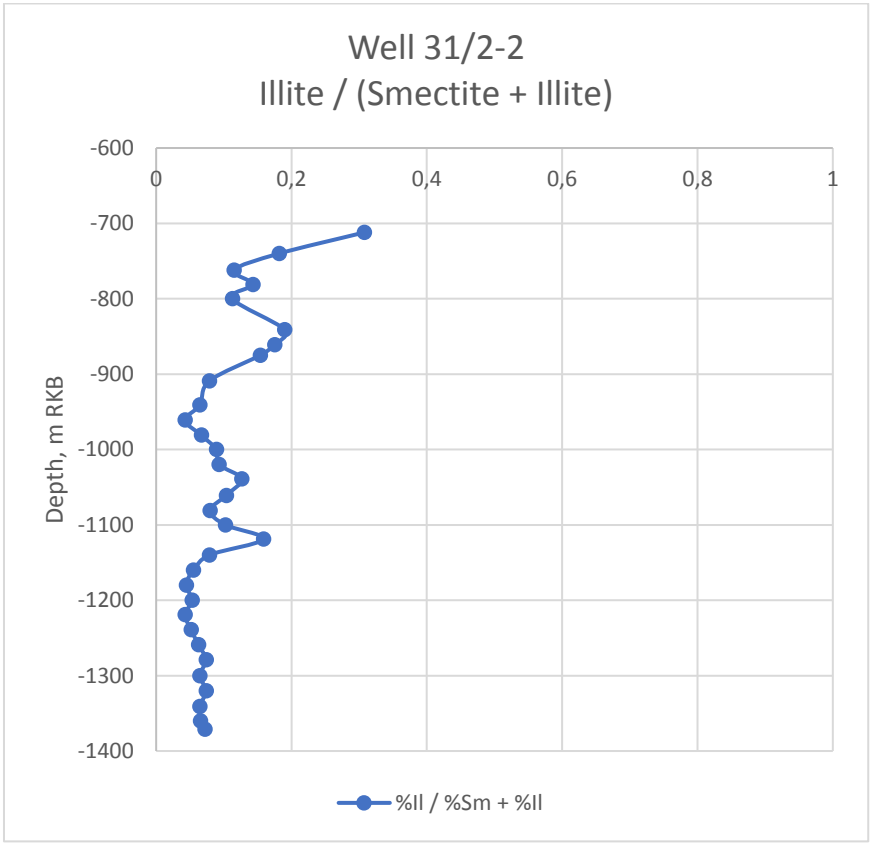

Figure 4-6: Graph displaying changes in the illite fraction of Smectite + Illite in each mineralogy sample from the well 30/3-3. Depth is measured from the well drilling floor (rotary kelly bushing).

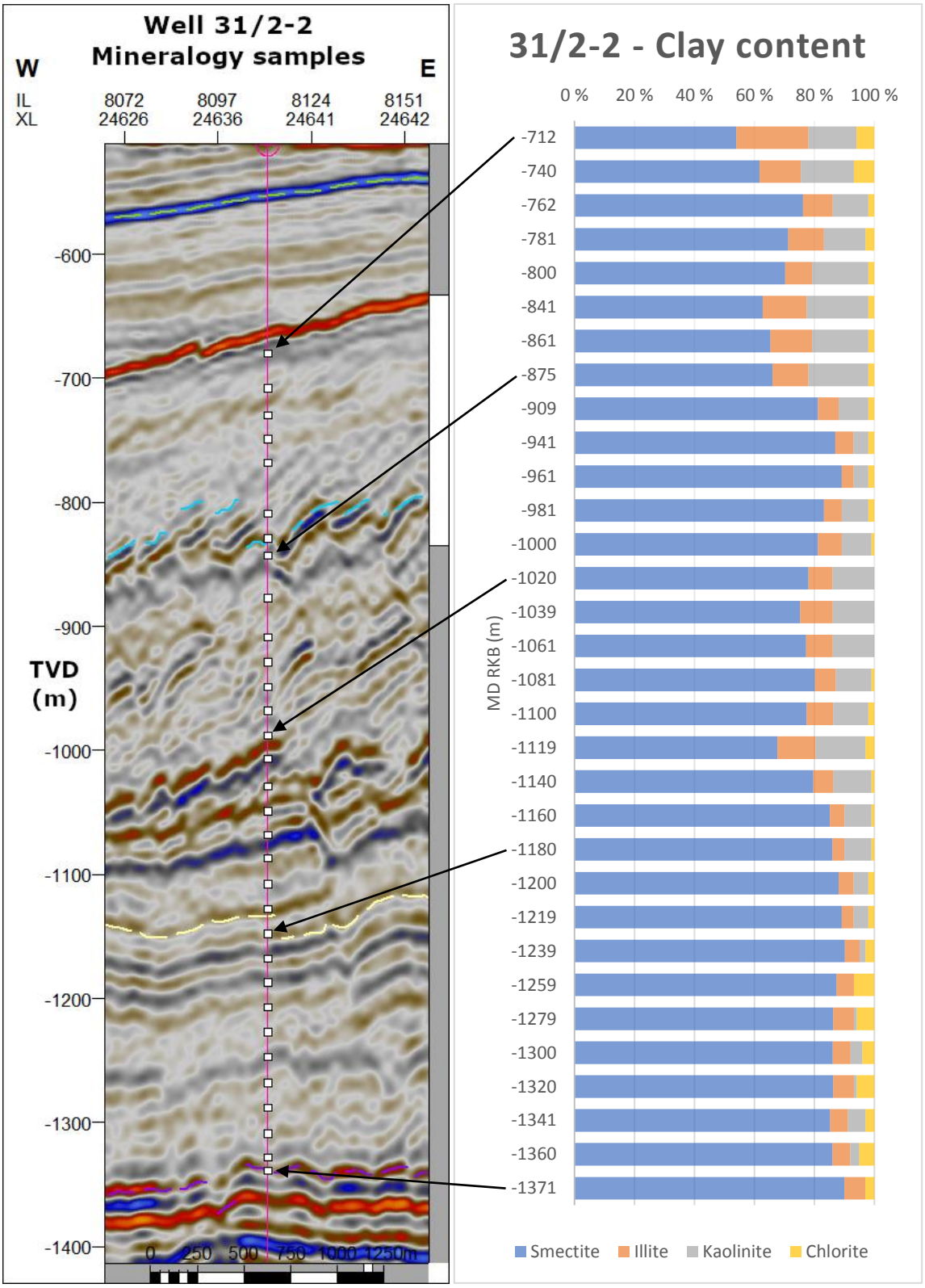

Figure 4-7: Seismic display of well 31/2-2 showing the depth of each sample (left), bar chart displaying clay content of samples (right). The left vertical axis is displayed in True Vertical Depth, the right vertical axis is displayed is measured depth from the well drilling floor (rotary kelly bushing).

4.1.5 Clay mineralogy of Well 31/3-1

This well shows lower fractions of smectite in the sequence above CSS-2. CSS-2 show a slight reduction in the amount of smectite from the top of the sequence downwards. From slightly above CSS-1, at the depth of -944 m and downwards, we see high values of smectite. Near the end of CSS-1 we observe a significant reduction in smectite content and increase in illite content (Figure 4-8).

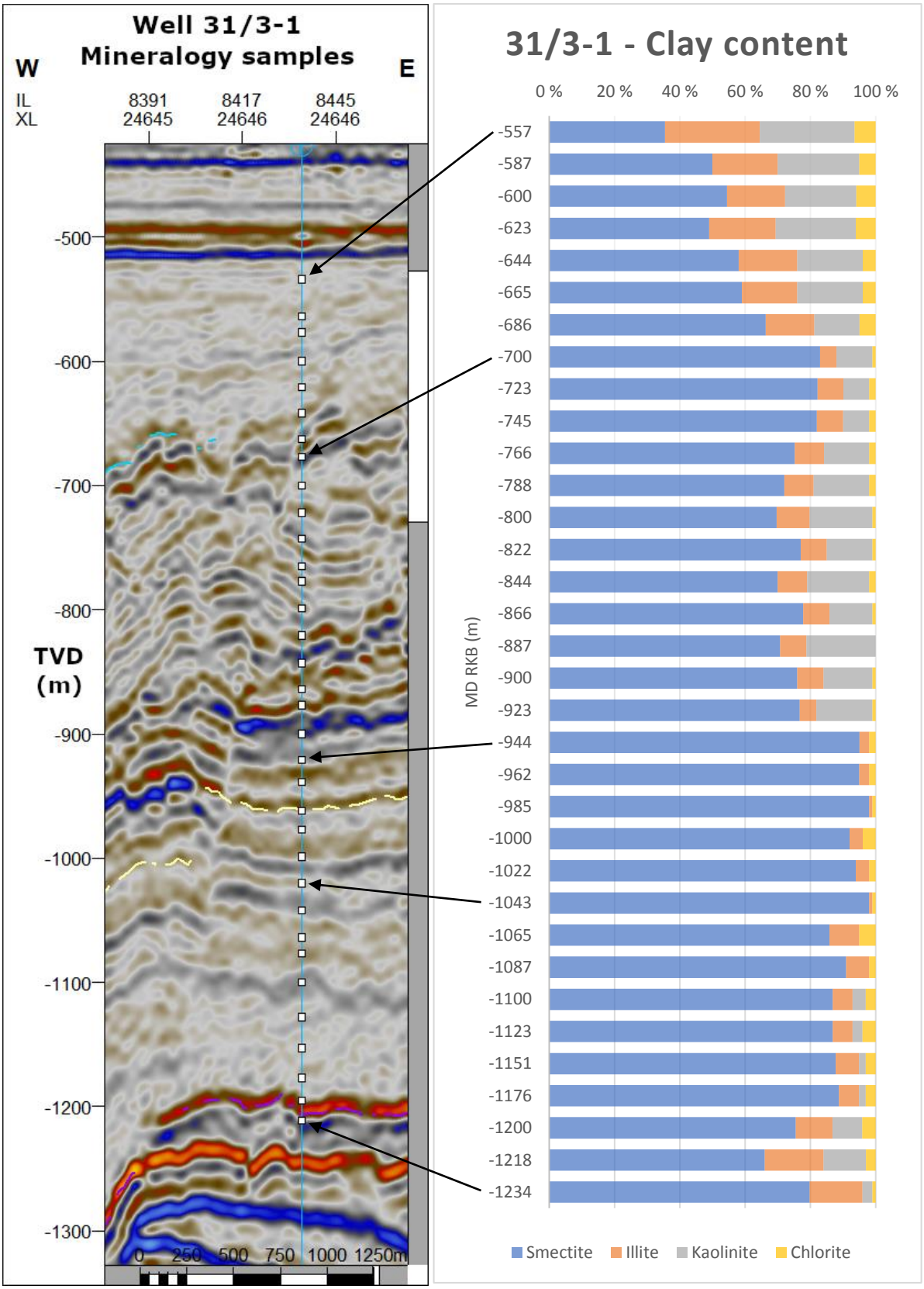

Figure 4-8: Seismic display of well 31/3-1 showing the depth of each sample (left), bar chart displaying clay content of samples (right). The left vertical axis is displayed in True Vertical Depth, the right vertical axis is displayed is measured depth from the well drilling floor (rotary kelly bushing).

4.1.6 Clay mineralogy of well 34/2-2

In this well we observe large amounts of glacial sediments with low fractions of smectite and high fractions of illite and chlorite. Starting from the top of CSS-4 at -1450 m, we observe a steady increase in the smectite fraction all the way down to the end of CSS-1 (Figure 4-9).

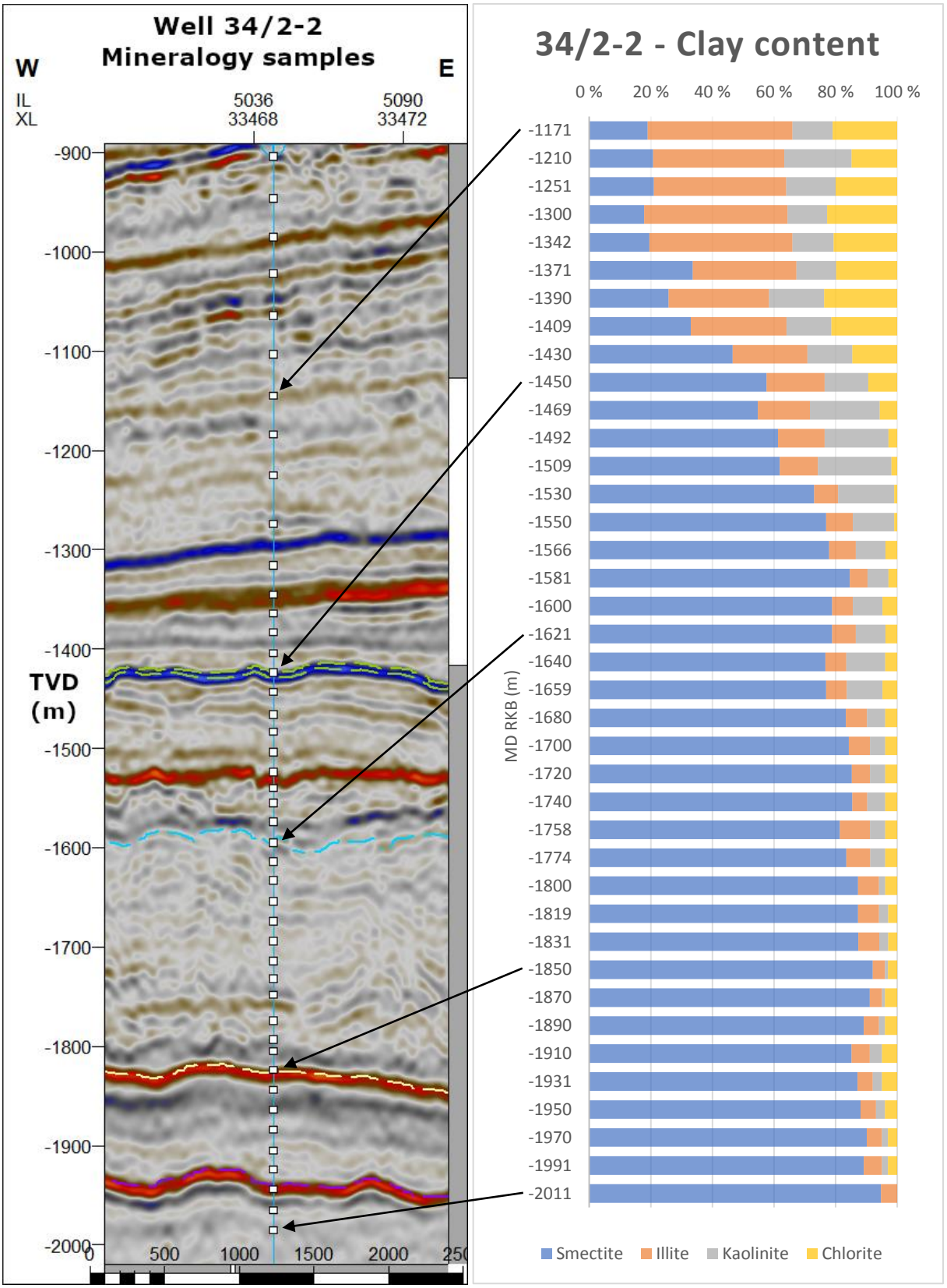

Figure 4-9: Seismic display of well 34/2-2 showing the depth of each sample (left), bar chart displaying clay content of samples (right). The left vertical axis is displayed in True Vertical Depth, the right vertical axis is displayed is measured depth from the well drilling floor (rotary kelly bushing).

4.1.7 Clay mineralogy of well 35/3-2

This well is located at the north-western part of the study area. The reflectors in this area are very chaotic, and that makes it difficult to find the CSS sequences here. Just above and below what we assume is Top Eocene (down to -1030), we observe reduces smectite fractions and elevated illite fractions compared to the rest of the well. The rest of the well show a very high smectite fraction around 87-93% (Figure 4-10).

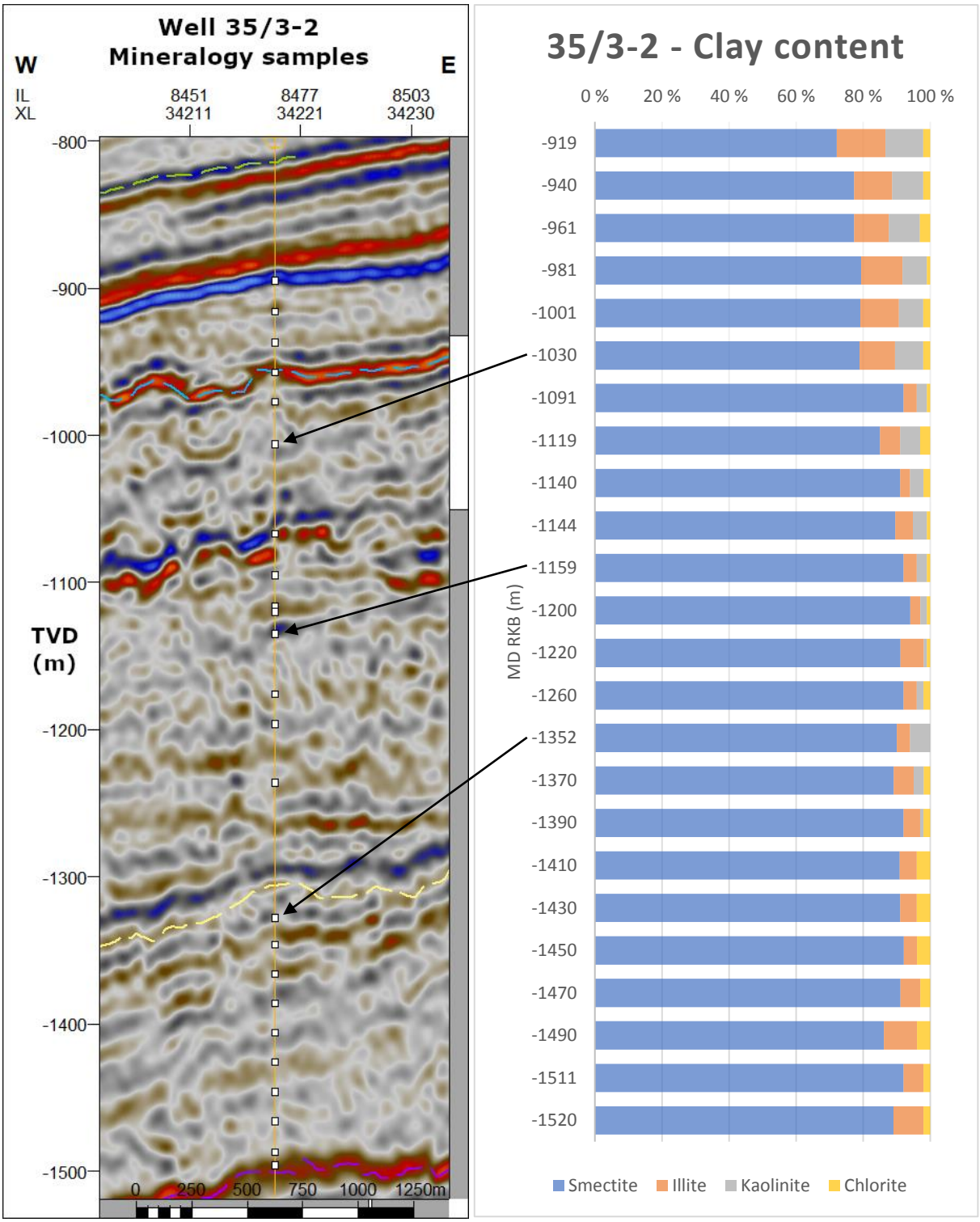

Figure 4-10: Seismic display of well 35/3-2 showing the depth of each sample (left), bar chart displaying clay content of samples (right). The left vertical axis is displayed in True Vertical Depth, the right vertical axis is displayed is measured depth from the well drilling floor (rotary kelly bushing).

4.2 Opal A – Opal-CT diagenetic reflectors & wireline logs

In these logs we attempt to spot and observe the changes in density caused by the Opal-A to Opal-CT transformation. We do this by measuring the average density of the well in sections above and below where we suspect Opal-A to CT transformation has occurred. We then use the average densities of these sections to calculate an estimated porosity, as explained in chapter 3.3.

4.2.1 Well log for 30/3-3

Figure 4-11 show two sections, above and below what is suspected to be the reflector indicating the transformation of Opal-A to Opal-CT. The average bulk density for the two sections marked in Figure 4-12 was calculated from the well log for 30/3-3.

The upper section has an average density of 1.86 g/cm^3. When calculated to an estimated porosity, we see this section has a porosity of 0.6838, or 68.4%.

The lower section has an average density of 2.02 g/cm^3. When calculated to an estimated porosity, we see this section has a porosity of 0.6250, or 62.5%.

The reduction in porosity from the upper to lower section is -0.0588, or -5.88%.

We also have mineralogy data proving the presence of Opal-CT the lower section (CSS-3). These are displayed as numbers next to the highlighted samples in the well. A value of e.g., 38 signify that 38% of the total amount of <6µm minerals present in the sample (Figure 4-11). The numbers we see in this well indicate the presence of large amounts of biogenic silica.

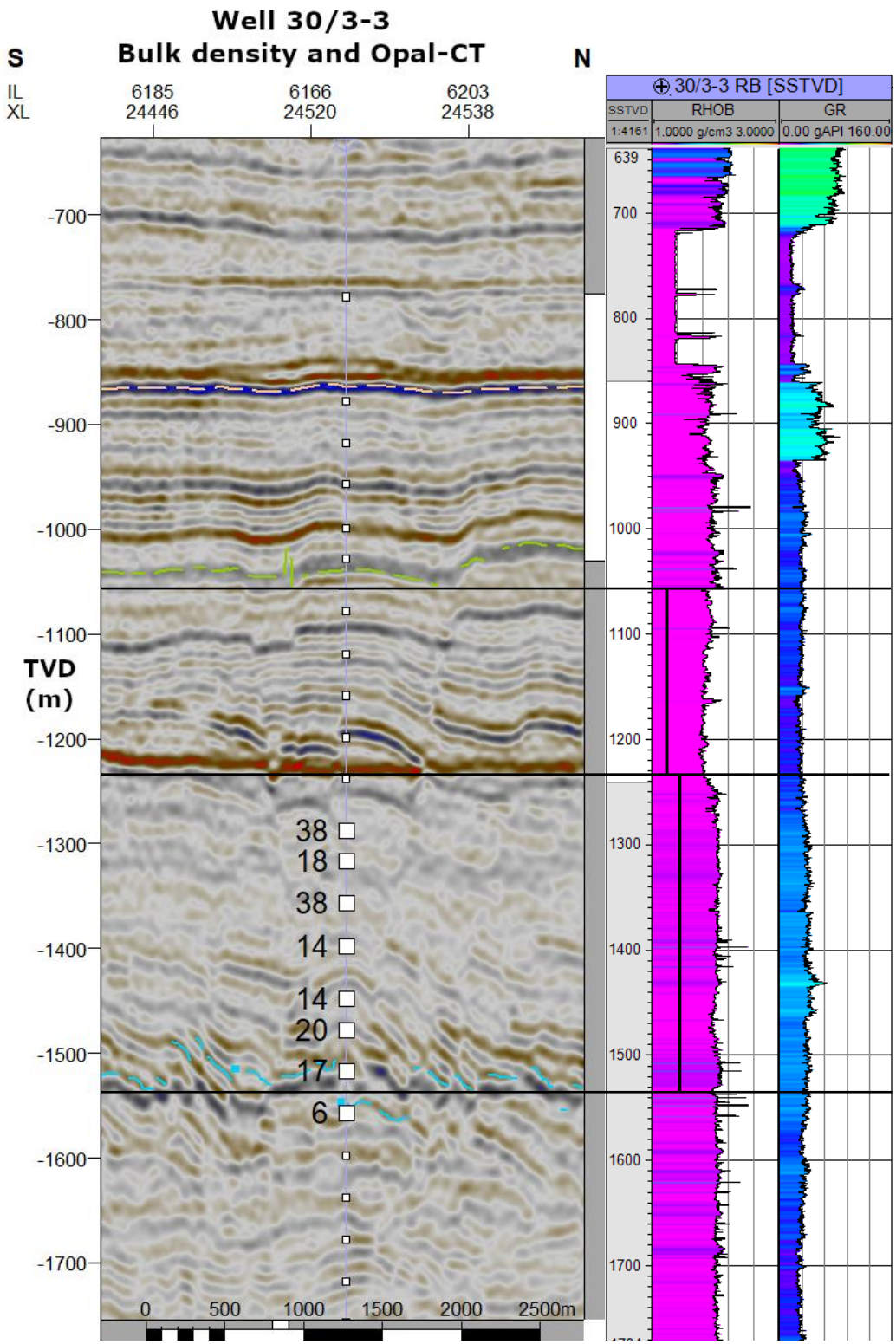

Figure 4-11: Mineralogy data showing the amounts of Opal-CT present in samples from well 30/3-3 (left), and well logs displaying gamma ray and bulk density logs for well 30/3-3 (right). The lines from the log to the seismic show the upper and lower sections that are being compared.

4.2.2 Well log for 31/2-5

Figure 4-12 show two sections, above and below what is suspected to be the reflector indicating the transformation of Opal-A to Opal-CT. The average bulk density for the two sections marked in Figure 4-12 was calculated from the well log for 31/2-5.

The upper section has an average density of 1.79 g/cm^3. When calculated to an estimated porosity, we see this section has a porosity of 0.7096, or 70.1%.

The lower section has an average density of 2.04 g/cm^3. When calculated to an estimated porosity, we see this section has a porosity of 0.6176, or 61.8%.

The reduction in porosity from the upper to lower section is -0.092, or -9.2%.

In this figure (Figure 4-12) we don't see as clear a diagenetic reflector as in 30/3-3, but it is the same sequence (CSS-3) just further east. The mineralogy data displayed on the highlighted samples in the well (Figure 4-12) show there are significant amounts of Opal-CT in the lower section (CSS-3). Polygonal faults are observed in the upper section (CSS-4), some of these faults appear to cross into the lower section (CSS-3).

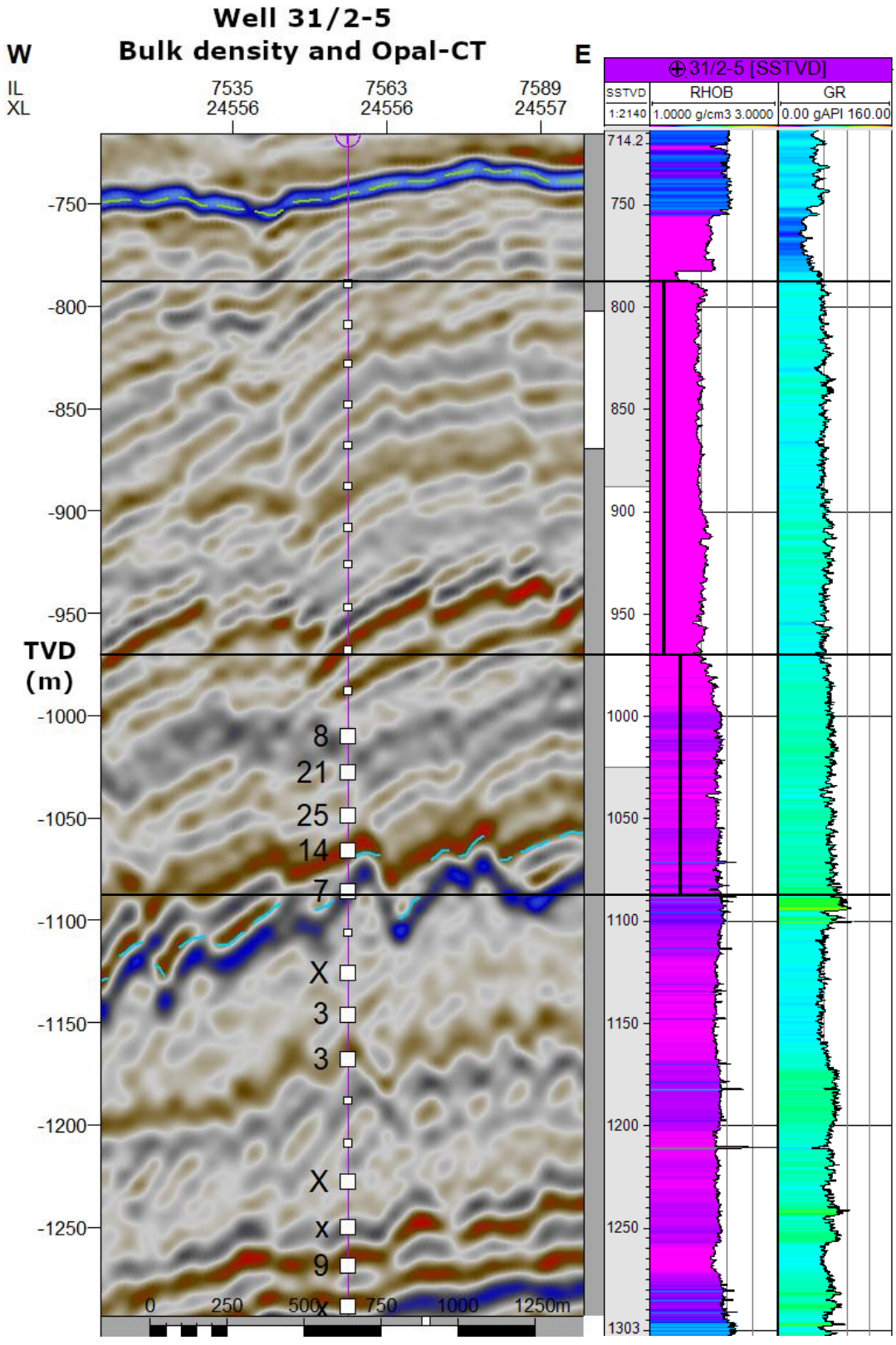

Figure 4-12: Mineralogy data showing the amounts of Opal-CT present in samples from well 31/2-5 (left), and well logs displaying gamma ray and bulk density logs for well 31/2-5 (right). The lines from the log to the seismic show the upper and lower sections that are being compared

4.2.3 Well log for 31/4-3

Figure 4-13 show two sections, above and below what is suspected to be the reflector indicating the transformation of Opal-A to Opal-CT. The average bulk density for the two sections marked in Figure 4-13 was calculated from the well log for 31/4-3.

The upper section has an average density of 1.84 g/cm^3. When calculated to an estimated porosity, we see this section has a porosity of 0.6912, or 69,1%.

The lower section has an average density of 2.01 g/cm^3. When calculated to an estimated porosity, we see this section has a porosity of 0.6287, or 62,9%.

The reduction in porosity from the upper to lower section is -0.0625, or -6.25%.

The reflector between the two sections in this will is quite small and fragmented sue to extensive polygonal faulting and sand injections (Figure 4-13). The upper section is mostly within the CSS-4 sequence, and the lower section is within the CSS-3 sequence. Polygonal faults can be observed in CSS-4, but not in the transparent CSS-3. Sand injections are however visible in CSS-3.

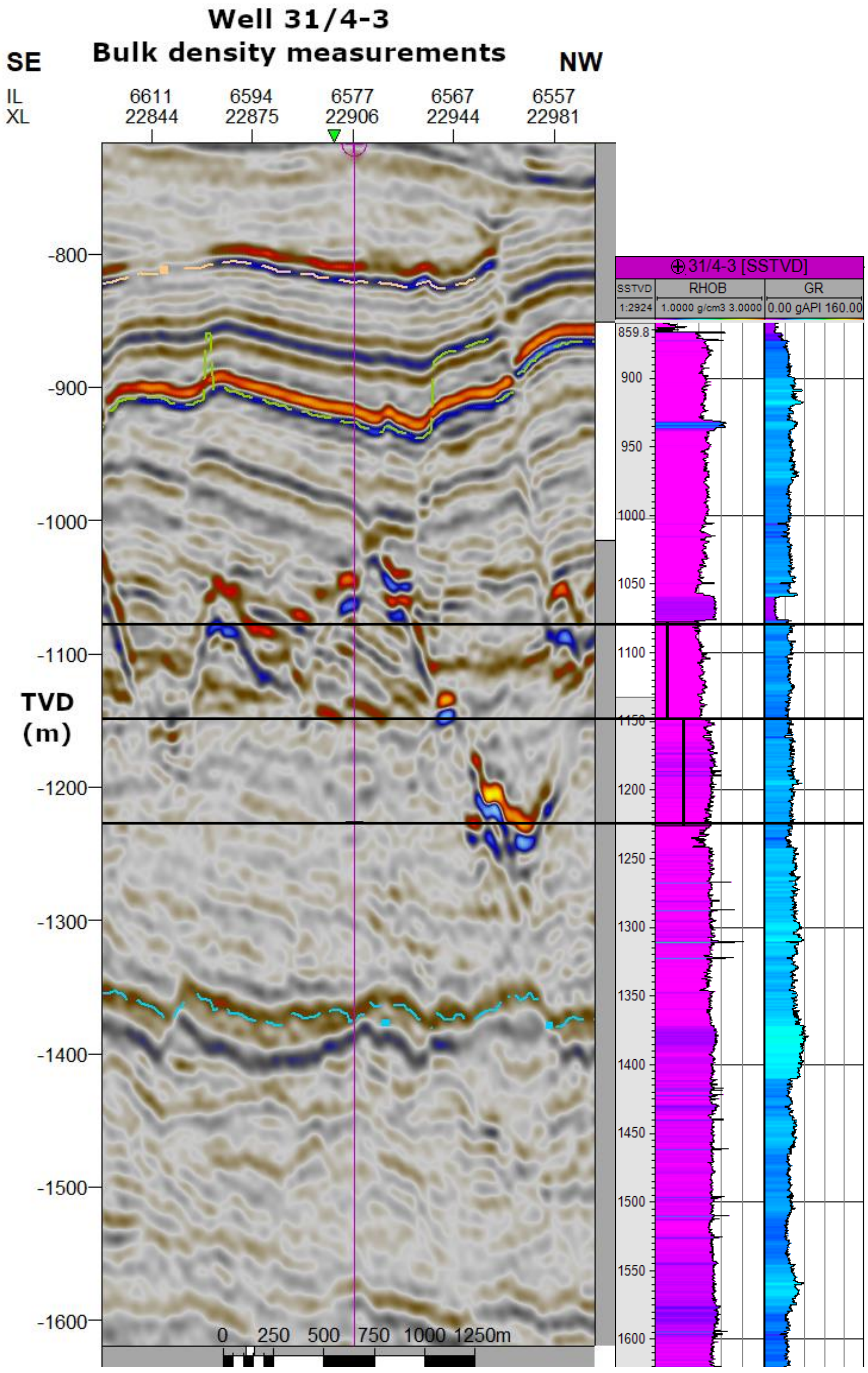

Figure 4-13: Well logs displaying gamma ray and bulk density logs for well 31/4-3. The lines from the log to the seismic show the upper and lower sections that are being compared

4.2.4 Well log for 35/11-3

Figure 4-14 show two sections, above and below what is suspected to be the reflector indicating the transformation of Opal-A to Opal-CT. The average bulk density for the two sections marked in Figure 4-14 was calculated from the well log for 31/2-5.

The upper section has an average density of 1.78 g/cm^3. When calculated to an estimated porosity, we see this section has a porosity of 0.7132, or 71.3%.

The lower section has an average density of 2.01 g/cm^3. When calculated to an estimated porosity, we see this section has a porosity of 0.6287, or 62.9%.

The reduction in porosity from the upper to lower section is -0.0845, or -8,45%.

Polygonal faults can be observed in the upper section (CSS-4). The lower section (CSS-3) is very transparent, and polygonal faults are not observed here.

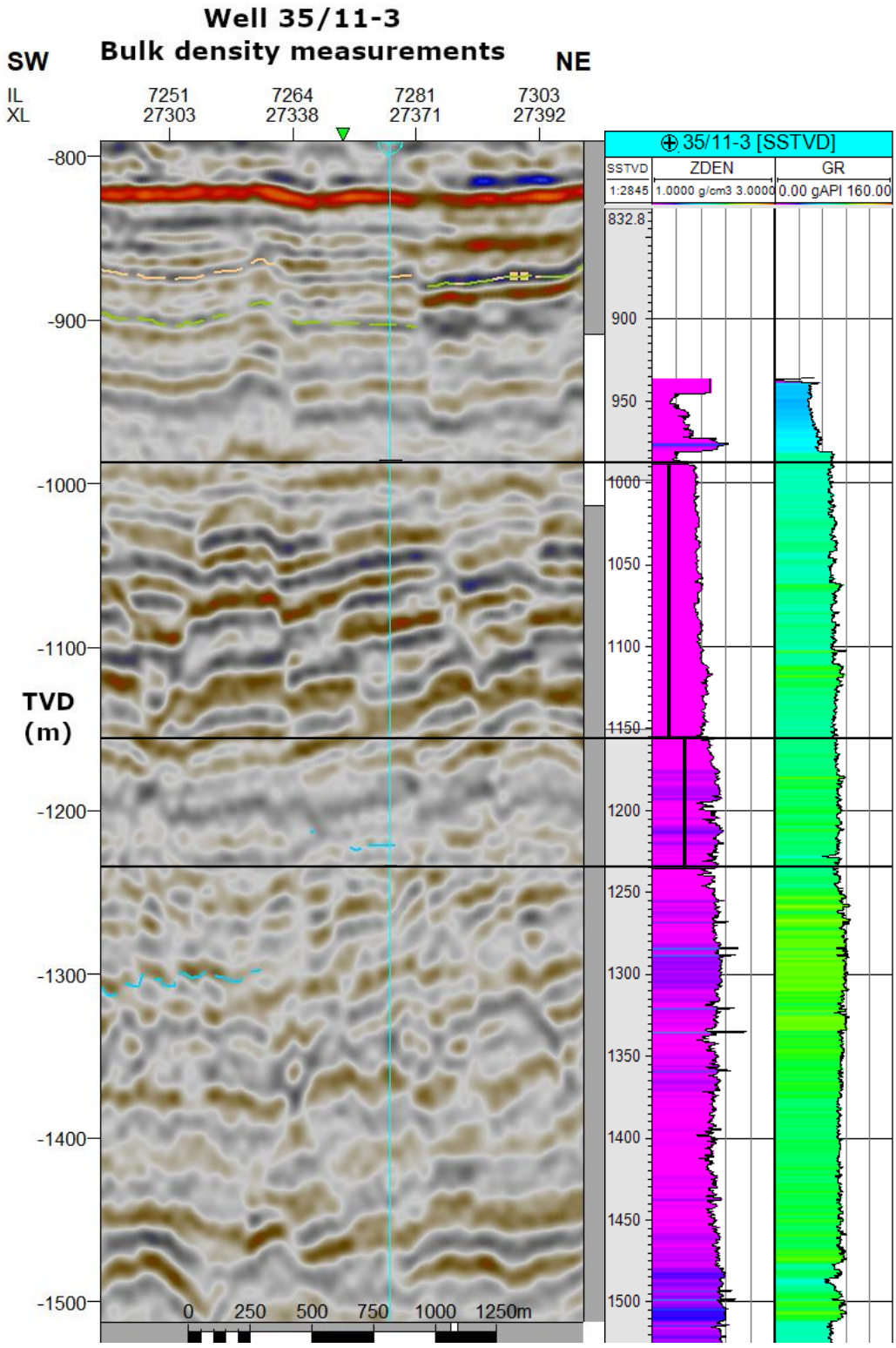

Figure 4-14: Well logs displaying gamma ray and bulk density logs for well 35/11-3. The lines from the log to the seismic show the upper and lower sections that are being compared

4.2.5 Well log for 31/2-1

This well log is not used to measure any porosities, but to highlight the measurements from the gamma ray log. For the previous four well log measurements, the gamma ray log did not show any large changes between the upper and lower sections, even though we observed significant changes in bulk density. In this well however, we see significant changes in the gamma ray log between CSS-4 and the sediments that appeared under this sequence after the CSS-3 onlap onto the flank. This indicates large mineralogical differences between CSS-4 and this new sequence underneath it (Figure 4-15).

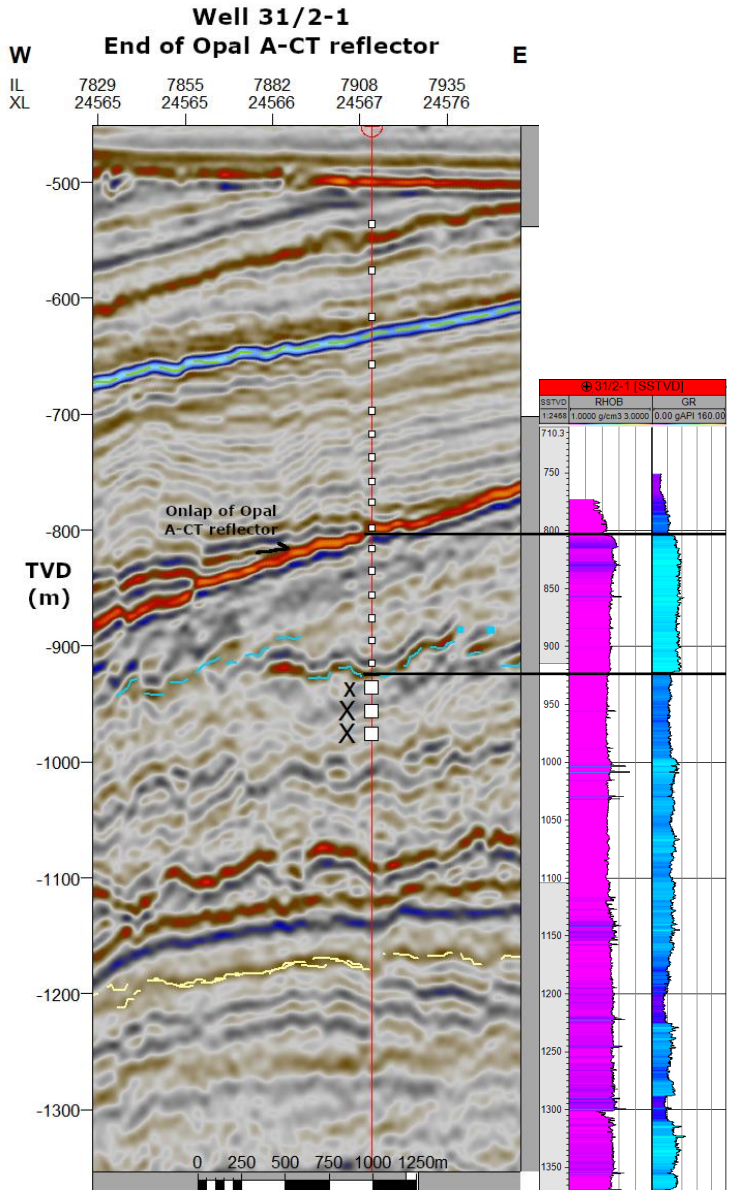

Figure 4-15: Gamma ray log measurement of CSS-4 and the sequence beneath it after CSS-3 onlap.

4.3 Seismic observations

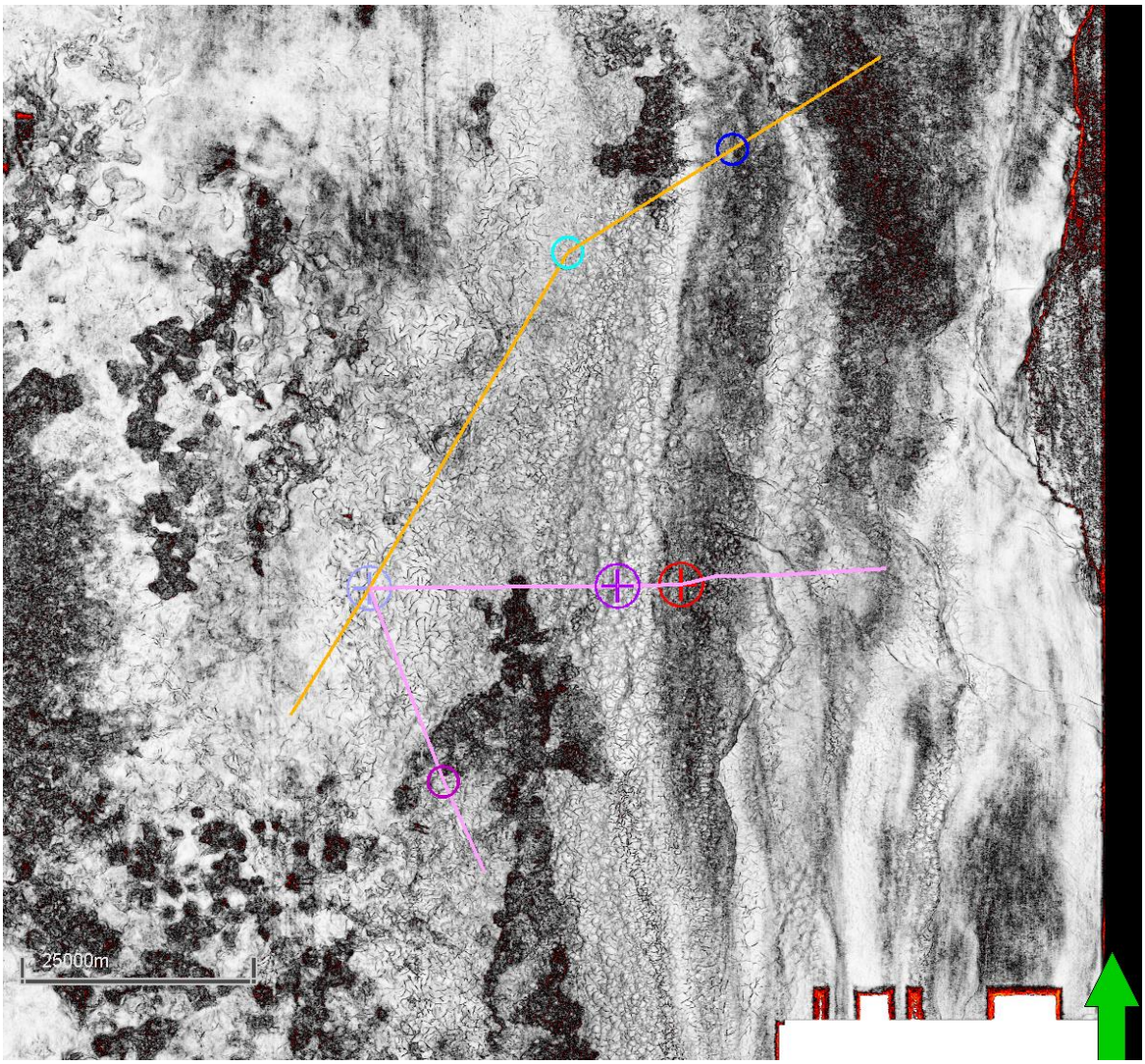

Figure 4-16: Variance map showing extensive polygonal faulting and the formation of mounds in the study area. The depth slice used for this variance map is at -980 m depth. The pink-colored line is seismic line 1, the orange line is seismic line 2.

At the end of the observations chapter, we will mention some of the observations made while working with the seismic in this study area, that might tie in with the mineralogy and well log data.

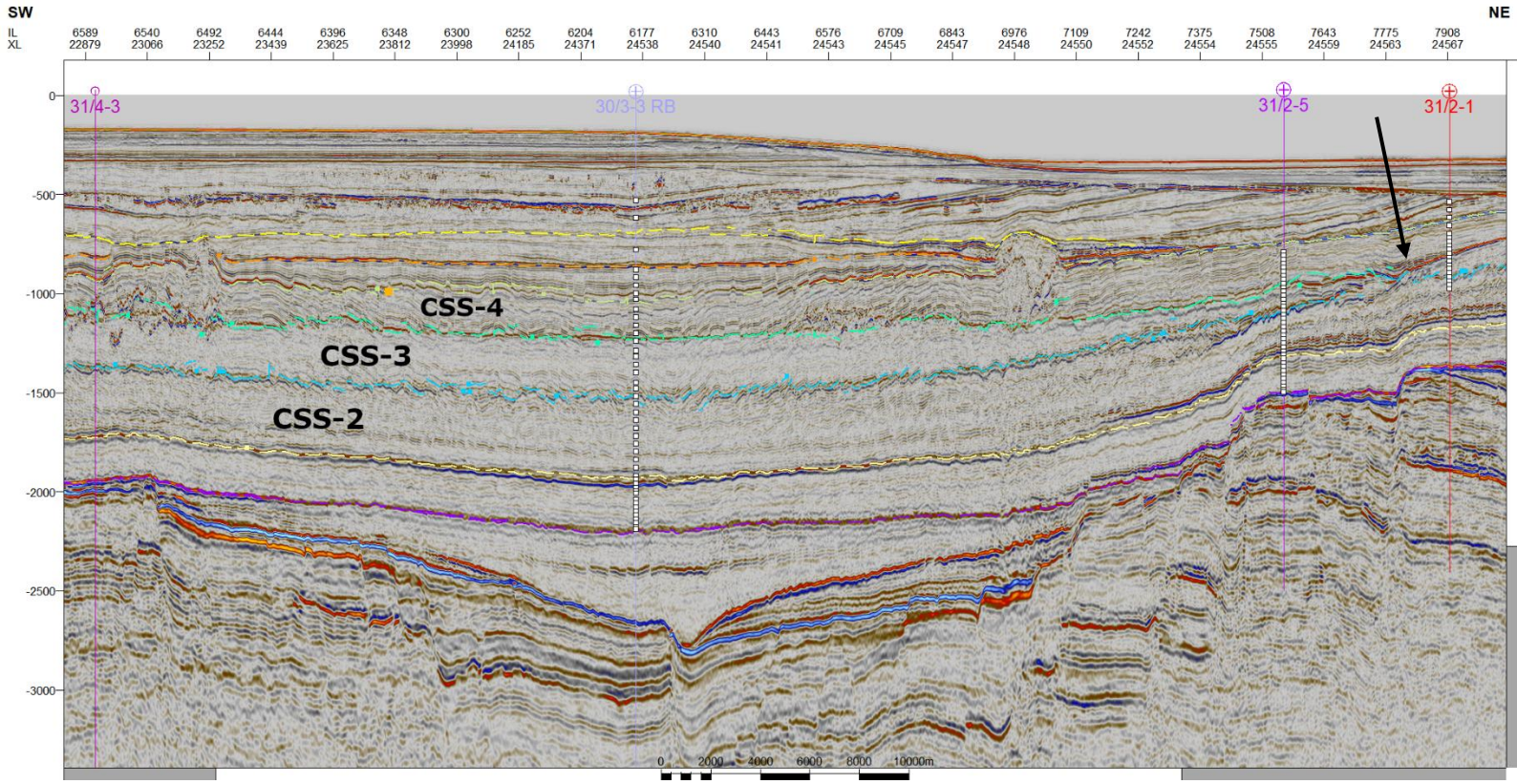

Figure 4-17: This seismic line crosses the wells 31/4-3, 30/3-3, 31/5-2, and 31/2-1.

4.3.1 Seismic line 1

The observations made in this area regarding polygonal faults, and to some extent sand mounds together with polygonal faults in the CSS-4 sequence, is that when we see prominent polygonal fault systems in CSS-4, it is always when the transparent sequence CSS-3 is situated underneath. When CSS-3 onlap and disappear on the basin flank (see arrow in Figure 4-17), the polygonal faults in CSS-4 disappear.

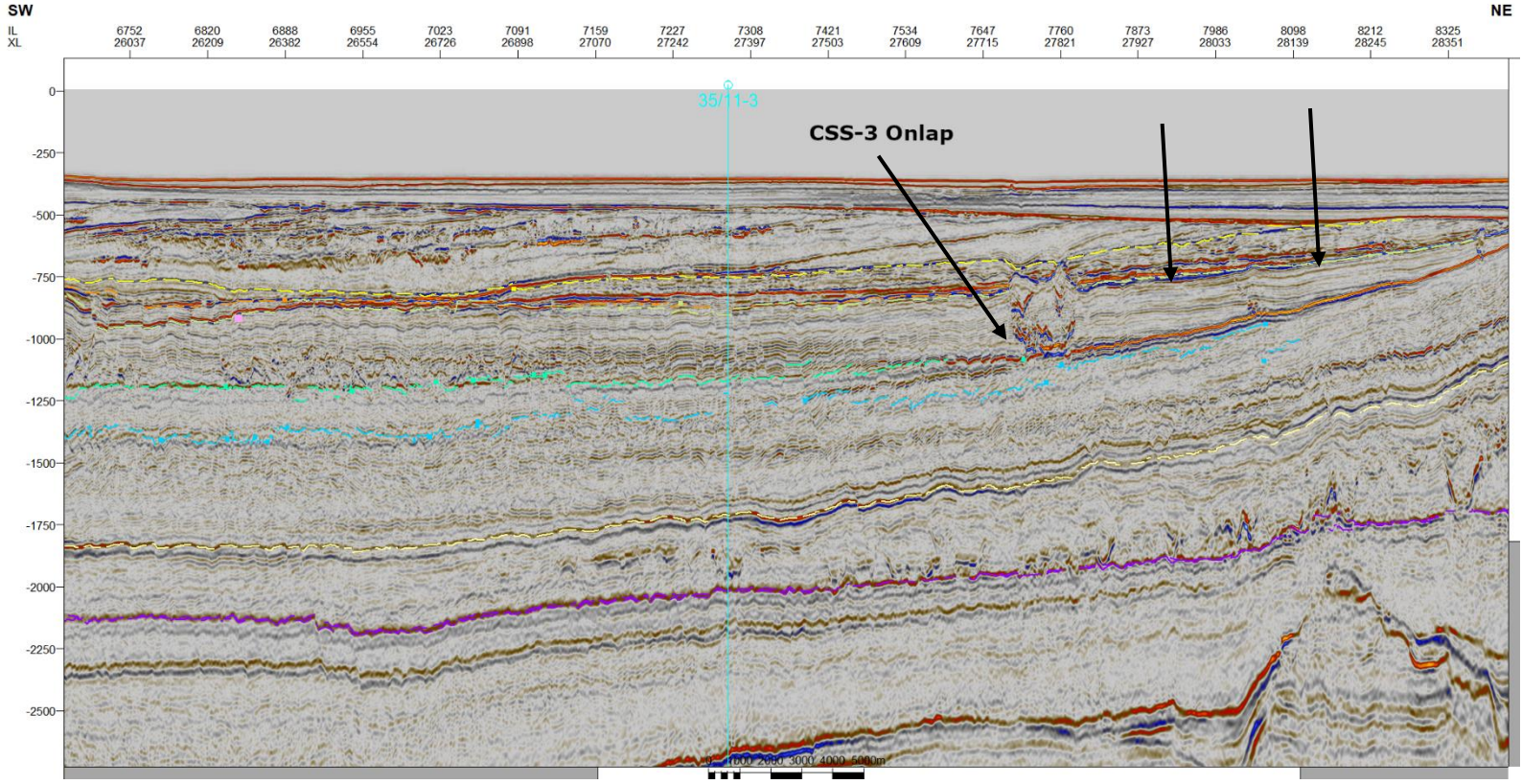

Figure 4-18: This seismic line crosses 35/11-3.

4.3.2 Seismic line 2

The same is observed in this seismic line, situated north of the first one (see Figure 4-16). When CSS-3 onlaps and disappears, it significantly changes the above CSS-4. The sequence changes from being severely deformed by polygonal faults, to having mostly horizontal and undisturbed reflectors (see arrows in Figure 4-18).

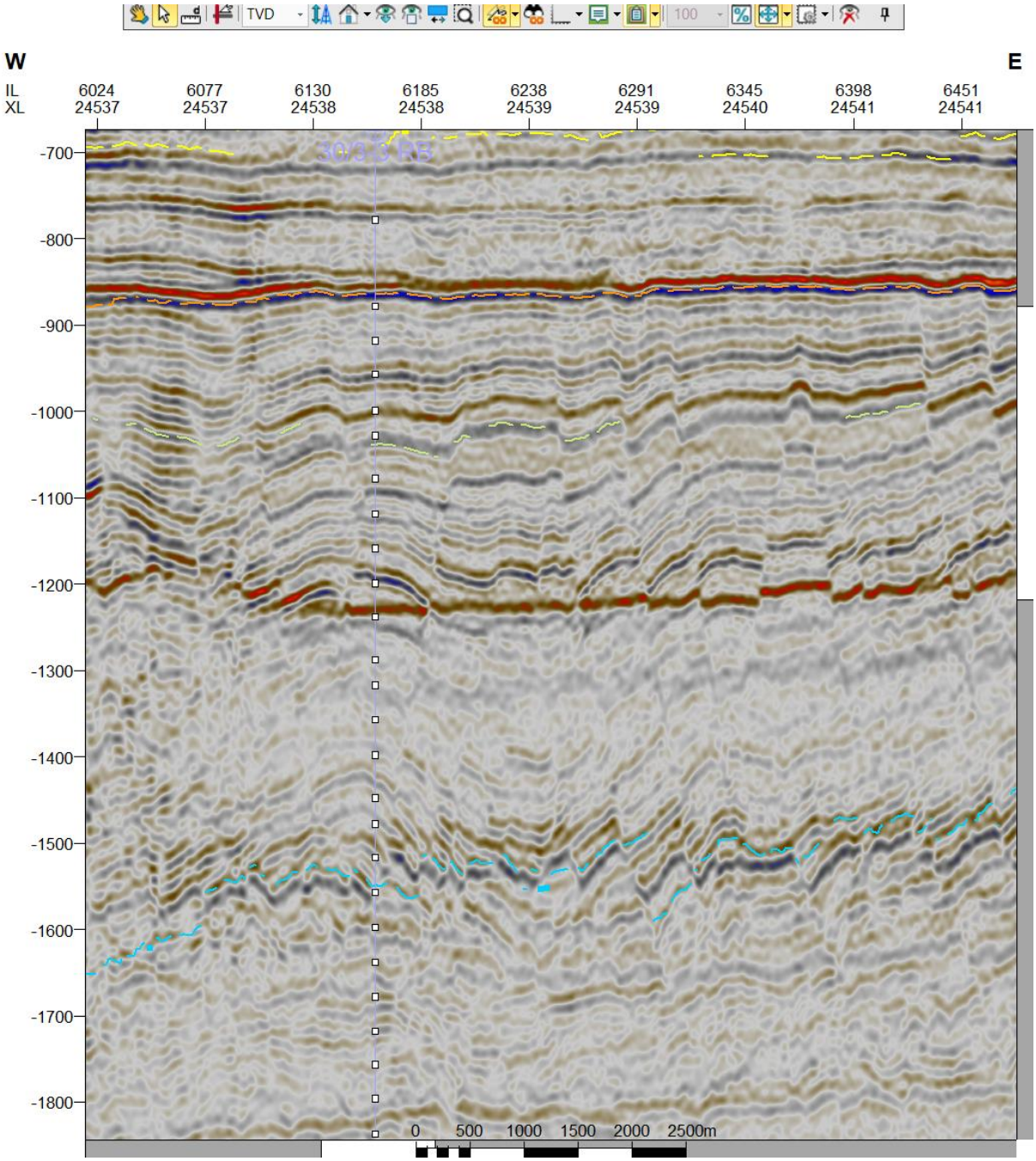

Figure 4.19: Seismic line crossing the well 30/3-3. What appears to be a diagenetic reflector crosscuts some of the overturned polygonal fault blocks.

4.3.3 Seismic line 3

Figure 4-19 shows the diagenetic reflector and the polygonal faults near the well 30/3-3.

5. Interpretation

When reviewing the mineralogy data, especially around the sequences CSS-3 and CSS-4, we do not find much evidence to support the proposition that contraction of the sediments in these areas are caused by smectite to illite transformation. In well 30/3-3 for instance, we see a slight increase in the smectite content from CSS-4 to CSS-3. But the fraction of illite either stays the same or is reduces compared to smectite. If smectite-illite transformation were to be responsible for the expansive polygonal fault systems observed in the Upper Oligocene sequence (CSS-4) we should be able to see a significant increase in the illite fraction. Since we do not, we consider this formation mechanism unlikely to be the cause of the PFS we see in the Upper Oligocene.

In well 30/3-3, we see what appears to be a diagenetic reflector. When measuring the average bulk density above and below this reflector, we note a large change in density. When calculated to an estimated porosity, we find that porosity is reduces by -5.88% going from CSS-4 above the reflector to CSS-3 below. Add to that the fact that mineralogy samples taken from the CSS-3 sequence reveal large amounts of Opal-CT in the samples. We see similar findings in well 31/2-5, and although we find less Opal-CT in the mineralogy samples here, the change in porosity going from CSS-4 to CSS-3 is -9.2%. We do not have mineralogy samples from the wells 31/4-3 and 35/11-3, but the measured porosity reduction at these wells is -6.25% and -8.45% respectively, it is not unreasonable to assume similar conditions in these wells as well.

Let us now consider why polygonal faulting does seem to occur in CSS-4 when CSS-3 has onlapped and disappeared. Assuming the polygonal faulting we see in the Upper Oligocene (CSS-4) sequence is the result of compaction and the release of pore fluids in the Lower Oligocene sequence (CSS-3), then it might explain why little to no polygonal faults appear in CSS-3 if CSS-4 is not situated below it.

If the Oligocene sequences contain biogenic silica, it might also explain why we see such a abrupt change in seismic facies going from CSS4 to CSS-3. Biogenic silica before transforming to Opal-CT would contribute to high porosity and low density in sediments, as the skeletal fragments of microorganisms contains a large amount of voids and pore space. Alternating layers of sediments with and without biogenic silica would be of different densities, and this difference might be possible to observe through seismic.

An example I would point to is the well 30/3-3. We know from mineralogy samples there is a lot of Opal-CT present, we also see what appears to be a very convincing diagenetic reflector between them. Looking closely at it in Figure 4-19 we see the diagenetic reflector is mostly horizontal despite the polygonal being offset. This suggests that the process is ongoing, and that there is biogenic silica in the sediments above the diagenetic reflector.

We can then theorize that biogenic silica is the cause of the strong contrast we see in the reflectors in the faulted sequence above the diagenetic. When this silica is transformed and the sediments compacted, this contrast is lowered, and we might get seismic facies more like the one we see under the diagenetic reflector at 30/3-3.

Neither the gamma ray logs, nor the clay mineralogy samples suggest a significant difference in lithology between the lower CSS-4 and upper CSS-3. This is best shown in the wells 30/3-3 and 31/2-5, where we also have confirmation that Opal-CT is present. The only lot that shows a significant difference is the bulk density log. This suggests the differences between CSS-3 and CSS-4, like the very easy to spot difference in seismic facies (see Figure 4.19), is not related to the clay mineralogy of the sequences but is instead caused by diagenetic alterations of biogenic silica.

As we see both similar seismic facies and similar reductions of porosity in both 31/4-3 and 35/11-3, we can suspect the same process takes place there as in well 30/3-3 and 31/2-5. These wells are quite far apart (see Figure 4-17) and we see from Figure 4-18 and Figure 4-19 that the seismic facies along CSS-4 and CSS-3, with polygonal faults in the upper sequence, a strong (possibly diagenetic) reflector at the sequence boundary, and a transparent sequence underneath, is seen everywhere in the study area around the wells 30/33, 31/2-5, 31/4-3 and 35/11-3. This might suggest that the process we observe within these four wells is at play over the whole study area.

6. Conclusion

- The Opal-A to Opal-CT transformation is very likely responsible for increasing bulk density and reduced porosity at the boundary between the Upper and Lower Oligocene sequences (CSS-4 and CSS-3)
- The smectite to illite transformation is unlikely to be related to polygonal faults in the study area, as significant increases in illite compared to smectite were not observed.
- The seismic facies of a faulted CSS-4 with a transparent CSS-3 underneath, can be seen through most parts of the study area.
- This suggests that biogenic silica and the Opal-A to Opal-CT transformation might play a large role in the formation of polygonal faults in the study area.

7. Future work

These are some possible avenues to expand upon the investigations regarding the influence biogenic silica seem to have on the formation of polygonal faults in the Oligocene sequences:

- Further investigations where more mineralogy data is available, both regarding clay mineralogy and biogenic silica.
- Better investigate the flanks to the basin and attempt to form a more cohesive explanation for why polygonal faults disappear near and on the margin.
- Map the seismic reflector between CSS-3 and CSS-4 and attempt to find more cases of possible diagenetic reflectors.

References

Cartwright, J.A. and Dewhurst, D.N. (1998) “Layer-bound compaction faults in fine-grained sediments,” Geological Society of America bulletin, 110(10), pp. 1242–1257.

Cartwright, J., James, D. and Bolton, A. (2003) “The genesis of polygonal fault systems: a review,” Geological Society special publication, 216(1), pp. 223–243.

Cartwright, J. (2011) “Diagenetically induced shear failure of fine-grained sediments and the development of polygonal fault systems,” Marine and petroleum geology, 28(9), pp. 1593–1610.

Faleide, J.I. et al. (2002) “Tectonic impact on sedimentary processes during Cenozoic evolution of the northern North Sea and surrounding areas,” Exhumation of the North Atlantic Margin: Timing, Mechanisms and Implications for Petroleum Exploration, 196(1), pp. 235–269.

Goulty, N.R. (2001) “Polygonal fault networks in fine-grained sediments – an alternative to the syneresis mechanism,” First break, 19(2), pp. 69–73.

Goulty, N.R. (2008) “Geomechanics of polygonal fault systems; a review,” Petroleum geoscience, 14(4), pp. 389–397.

Henriet, J.P., De Batist, M., Van Vaerenbergh, W. & Verschuren, M. 1989. Seismic facies and clay tectonic features in the southern North Sea. Bulletin of the Belgian Geological Society, 97, 457-472

Henriet, J.P., De Batist, M. & Verschuren, M. 1991. Early fracturing of Palengene clays, southernmost North Sea: relevance to mechanisms of primary hydrocarbon migration. In: Spencer, A.M. (ed.) Generation, accumulation and production of Europe's hydrocarbons. Special Publication of the European Association of Petroleum Geologists, 1, 217-227

Hermanrud, C. and Undertun, O. (2019) “Resolution limits of fluid overpressures from mineralogy, porosity, and sonic velocity variations in North Sea mudrocks,” AAPG bulletin, 103(11), pp. 2665–2695.

Higgs, W.G. and McClay, K.R. (1993) “Analogue sandbox modelling of Miocene extensional faulting in the Outer Moray Firth,” Geological Society special publication, 71(1), pp. 141–162.

Jordt, H. et al. (1995) “Cenozoic sequence stratigraphy of the central and northern North Sea Basin: tectonic development, sediment distribution and provenance areas,” Marine and petroleum geology, 12(8), pp. 845–879.

Jordt, H., Thyberg, B.I. and Nottvedt, A. (2000) “Cenozoic evolution of the central and northern North Sea with focus on differential vertical movements of the basin floor and surrounding clastic source areas,” Dynamics of the Norwegian Margin, 167(1), pp. 219–243.

Kastner, M., Keene, J.B. and Gieskes, J.M. (1977) “Diagenesis of siliceous oozes—I. Chemical controls on the rate of opal-A to opal-CT transformation—an experimental study,” Geochimica et cosmochimica acta, 41(8), pp. 1041,1053–1051,1059.

Norwegian Petroleum Directorate (2023) DISKOS / About us. Available at: https://www.npd.no/en/diskos/About/ (Accessed: 11 May 2023)

Rundberg, Y. (1991) Tertiare sedimentary history and basin evolution of the Norwegian North Sea between 60 – 60 N – an integrated approach

Shin, H., Santamarina, J., & Cartwright, J. (2008). Contraction-driven shear failure in compacting uncemented sediments. Geology (Boulder), 36(12), 931-934

Thyberg, B.I. et al. (1999) “Upper Oligocene diatomaceous deposits in the northern North Sea - silica diagenesis and paleogeographic implications,” Norsk Geologisk Tidsskrift, 79(1), pp. 3–18.

Ziegler, P.A. (1975) “Geologic evolution of North Sea and its tectonic framework,” AAPG bulletin, 59(7), pp. 1073–1097.